Kaunas University of Technology

Faculty of Mechanical Engineering and Design

Small Unmanned Aerial Vehicle Stability Analysis

Master's Final Degree Project

Artem Shevchenko

Project author

Assoc. Prof. Saulius Japertas

Supervisor

Kaunas, 2026

Kaunas University of Technology

Faculty of Mechanical Engineering and Design

Small Unmanned Aerial Vehicle Stability Analysis

Master's Final Degree Project

Aeronautical Engineering (6211EX024)

Artem Shevchenko

Project author

Assoc. Prof. Saulius Japertas

Supervisor

Prof. Laurencas Raslavičius

Reviewer

Kaunas, 2026

Kaunas University of Technology

Faculty of Mechanical Engineering and Design

Artem Shevchenko

Small Unmanned Aerial Vehicle Stability Analysis

Declaration of Academic Integrity

I confirm the following:

1. I have prepared the final degree project independently and honestly without any violations of the copyrights or other rights of others, following the provisions of the Law on Copyrights and Related Rights of the Republic of Lithuania, the Regulations on the Management and Transfer of Intellectual Property of Kaunas University of Technology (hereinafter – University) and the ethical requirements stipulated by the Code of Academic Ethics of the University;

2. All the data and research results provided in the final degree project are correct and obtained legally; none of the parts of this project are plagiarised from any printed or electronic sources; all the quotations and references provided in the text of the final degree project are indicated in the list of references;

3. I have not paid anyone any monetary funds for the final degree project or the parts thereof unless required by the law;

4. I understand that in the case of any discovery of the fact of dishonesty or violation of any rights of others, the academic penalties will be imposed on me under the procedure applied at the University; I will be expelled from the University and my final degree project can be submitted to the Office of the Ombudsperson for Academic Ethics and Procedures in the examination of a possible violation of academic ethics.

Artem Shevchenko

Confirmed electronically

Kaunas University of Technology

Faculty of Mechanical Engineering and Design

Task of the Master's Final Degree Project

Given to the student – Artem Shevchenko

1. Topic of the project

Small Unmanned Aerial Vehicle Stability Analysis

(In English)

Mažojo bepiločio orlaivio stabilumo analizė

(In Lithuanian)

2. Aim and tasks of the project

Aim: To perform static and dynamic stability analysis and optimization of a small fixed-wing UAV, including center of gravity, dynamic modes assessment and improvement of longitudinal and lateral-directional characteristics using numerical aerodynamic tools.

Tasks:
1. Perform a research on mass and balance and static-dynamic stability of a small fixed-wing UAV.
2. Define a benchmark UAV for further analysis.
3. Determine the neutral point, static margin, and design allowable CG envelope.
4. To evaluate longitudinal static stability for different CG positions.
5. Perform an analysis of longitudinal and lateral-directional dynamic stability modes.
6. Based on analysis, propose design improvements for enhancing weak stability modes and overall flight behaviour.
7. Perform a static stability analysis validation in high fidelity CFD.

3. Main requirements and conditions

Maximum Take-Off Mass: 5 kg
Maximum wingspan: 2 m
Minimum stall velocity: 10 m/s

4. Additional requirements and conditions for the project, report and appendices

Not applicable

Project author	Artem Shevchenko		15-02-2026
	(Name, Surname)		*(Date)*
Supervisor	Saulius Japertas		15-02-2026

	(Name, Surname)	*(Date)*
Head of study field programs	Artūras Keršys	15-02-2026
	(Name, Surname)	*(Date)*

Shevchenko, Artem. Small Unmanned Aerial Vehicle Stability Analysis. Master's Final Degree Project / supervisor assoc. prof. Saulius Japertas; Faculty of Mechanical Engineering and Design, Kaunas University of Technology.

Study field and area (study field group): Aeronautical Engineering (E14), Engineering Science.

Keywords: UAV, Stability Analysis, mass and balance, CG.

Kaunas, 2026. 57 pages

Summary

This final degree project presents a preliminary static and dynamic stability analysis of a small fixed-wing unmanned aerial vehicle. The analysed UAV is limited by the main project requirements: maximum take-off mass of 5 kg, maximum wingspan of 2 m and stall velocity of 10 m/s. The aim of the work is to evaluate the influence of centre of gravity position on longitudinal and lateral-directional stability and to define the allowable CG envelope for the benchmark UAV configuration.

The research includes a review of mass and balance principles, static stability, dynamic stability modes and numerical tools suitable for light UAV stability analysis. The benchmark aircraft geometry was defined using preliminary aircraft sizing relations and tail volume coefficient methodology. The final configuration includes a rectangular main wing, horizontal tail plane and vertical tail plane. FLOW5 was selected as the main numerical tool for aerodynamic and stability analysis.

A component-based mass and balance model was prepared. The initial centre of gravity position was obtained at 25.1% MAC. Based on the pitching moment curve, the neutral point was calculated as 50.8% MAC and the initial static margin was 25.7% MAC. Using the selected static margin range of 20–25% MAC, the allowable CG envelope was defined as 25.8–30.8% MAC. Three CG positions were analysed: 25.8%, 28.3% and 30.8% MAC.

The results showed that the benchmark UAV is longitudinally statically stable for all investigated CG positions. Dynamic stability analysis showed that the short-period, phugoid, roll subsidence and Dutch roll modes are dynamically stable. The short-period mode recovered in less than 2 seconds, roll subsidence recovered in less than 0.2 seconds and Dutch roll recovered in less than 3 seconds. The phugoid mode was stable but lightly damped, with recovery time to 10% amplitude between 92 and 165 seconds.

A limited high-fidelity CFD validation was also performed in Ansys Fluent for the forward CG position of 25.8% MAC. The CFD results confirmed the same longitudinal static stability trend as FLOW5, since the pitching moment coefficient decreased with increasing lift coefficient. Therefore, the benchmark UAV can be considered longitudinally statically stable within the investigated CG range.

Shevchenko, Artem. Mažojo bepiločio orlaivio stabilumo analizė. Magistro baigiamasis projektas / doc. Saulius Japertas; Kauno technologijos universitetas, Mechanikos inžinerijos ir dizaino fakultetas.

Studijų kryptis ir sritis (studijų krypčių grupė): Aeronautikos inžinerija (E14), Inžinerijos mokslai.

Reikšminiai žodžiai: bepilotis orlaivis, stabilumo analizė, masė ir balansas, sunkio centras.

Kaunas, 2026. 57 p.

Santrauka

Šiame baigiamajame studijų projekte pateikiama preliminari mažo fiksuoto sparno bepiločio orlaivio statinio ir dinaminio stabilumo analizė. Analizuojamas bepilotis orlaivis yra apribotas pagrindiniais projekto reikalavimais: didžiausia kilimo masė – 5 kg, didžiausiu sparnų mojumi – 2 m ir smukos greičiu – 10 m/s. Darbo tikslas – įvertinti sunkio centro padėties įtaką išilginiam ir šoniniam-kryptiniam stabilumui bei nustatyti leistiną sunkio centro diapazoną bazinės bepiločio orlaivio konfigūracijos atveju.

Tyrime apžvelgiami masės ir balanso principai, statinis stabilumas, dinaminio stabilumo režimai ir skaitmeniniai įrankiai, tinkami lengvųjų bepiločių orlaivių stabilumo analizei. Bazinio orlaivio geometrija buvo apibrėžta naudojant preliminarius orlaivio dydžio nustatymo ryšius ir uodegos tūrio koeficiento metodiką. Galutinę konfigūraciją sudaro stačiakampis pagrindinis sparnas, horizontalioji uodegos plokštuma ir vertikalioji uodegos plokštuma. FLOW5 buvo pasirinkta kaip pagrindinė skaitmeninė aerodinaminės ir stabilumo analizės priemonė.

Buvo parengtas komponentais pagrįstas masės ir balanso modelis. Pradinė sunkio centro padėtis buvo nustatyta ties 25,1 % VAS. Remiantis išilginio momento kreive, neutralusis taškas buvo apskaičiuotas ties 50,8 % VAS, o pradinė statinė atsarga sudarė 25,7 % VAS. Naudojant pasirinktą 20–25 % VAS statinės atsargos intervalą, leistinas sunkio centro diapazonas buvo nustatytas kaip 25,8–30,8 % VAS. Buvo analizuojamos trys sunkio centro padėtys: 25,8 %, 28,3 % ir 30,8 % VAS.

Rezultatai parodė, kad bazinis bepilotis orlaivis yra išilgai statiškai stabilus visose tirtose sunkio centro padėtyse. Dinaminio stabilumo analizė parodė, kad trumpojo periodo, fugoido, riedėjimo slopinimo ir olandiškojo svyravimo režimai yra dinamiškai stabilūs. Trumpojo periodo režimas nuslopdavo greičiau nei per 2 sekundes, riedėjimo slopinimas – greičiau nei per 0,2 sekundės, o olandiškasis svyravimas – greičiau nei per 3 sekundes. Fugoido režimas buvo stabilus, tačiau silpnai slopinamas, o atsistatymo iki 10 % amplitudės trukmė siekė nuo 92 iki 165 sekundžių.

Ribota aukšto tikslumo CFD validacija taip pat buvo atlikta naudojant Ansys Fluent, esant priekinei sunkio centro padėčiai 25,8 % VAS. CFD rezultatai patvirtino tą pačią išilginio statinio stabilumo tendenciją kaip ir FLOW5, nes išilginio momento koeficientas mažėjo didėjant keliamosios jėgos koeficientui. Todėl galima teigti, kad bazinis bepilotis orlaivis yra išilgai statiškai stabilus tirtame sunkio centro diapazone.

Table of contents

List of figures

List of tables

List of abbreviations and terms

Abbreviations

AoA – Angle of Attack
AR – Aspect Ratio
AVL – Athena Vortex Lattice
BEM – Basic Empty Mass
CAD – Computer-Aided Design
CFD – Computational Fluid Dynamics
CG – Center of Gravity
L – Lift (lifting force)
D – Drag (drag force)
M – Moment
M_z – Pitching Moment
C_L – Lift Coefficient
C_D – Drag Coefficient
C_m – Pitching Moment Coefficient
Cl – Rolling Moment Coefficient
Cn – Yawing Moment Coefficient
DOM – Dry Operating Mass
HTP – Horizontal Tail Plane
ISA – International Standard Atmosphere
LLT – Lifting-Line Theory
MAC – Mean Aerodynamic Chord
MTOM – Maximum Take-Off Mass
NP – Neutral Point
OM – Operating Mass
SM – Static Margin
TOM – Take-Off Mass
UAV – Unmanned Aerial Vehicle
VLM – Vortex Lattice Method
V_{ne} – Never Exceed Speed
V_C – Cruise Speed
V_S – Stall Speed
p – Pressure
VTP – Vertical Tail Plane
ZFM – Zero-Fuel Mass

Introduction

When designing a UAV it is very important to consider not only aerodynamics performance in terms of obtaining C_L vs AOA, C_D vs AOA, C_L/C_D curves and estimating the important speed, optimum cruise altitude and flight range. It is very important to take into account mass and balance, static and dynamic stability.

Knowing an aircraft's mass and balance as well as its static and dynamic stability is very crucial in flight, as it gives an understanding how the aircraft behaves in flight, how it reacts to disturbances (for example a wind gust), if it returns to the equilibrium state and how fast. As well as it gives a full picture of the center of gravity limits.

These characteristics directly influence the ability of the aircraft to maintain stable and predictable flight conditions, which is particularly important for light UAVs, where even small control inputs or minor changes in mass distribution can have a significant effect on flight behaviour.

While mentioning small UAVs, it is understandable that due to their low mass and high sensitivity to disturbances, ensuring stable and predictable flight behaviour is essential. Therefore, detailed analysis of mass distribution, center of gravity and stability characteristics is critically important for safe and efficient UAV operation.

The novelty of this work lies in the combined analysis of static and dynamic stability of a small fixed-wing UAV with limited MTOM of 5 kg, maximum wingspan of 2 m and stall velocity of 10 m/s using modern numerical tools.

The aim of the project is to perform static and dynamic stability analysis and optimization of a small fixed-wing UAV, including center of gravity, dynamic modes assessment and improvement of longitudinal and lateral-directional characteristics using numerical aerodynamic tools.

Tasks:
1. Perform a research on mass and balance and static-dynamic stability of a small fixed-wing UAV.
2. Define a benchmark UAV for further analysis.
3. Determine the neutral point, static margin, and design allowable CG envelope.
4. To evaluate longitudinal static stability for different CG positions.
5. Perform an analysis of longitudinal and lateral-directional dynamic stability modes.
6. Based on analysis, propose design improvements for enhancing weak stability modes and overall flight behaviour.
7. Perform a static stability analysis validation in high fidelity CFD.

1. Mass and Balance of Aircraft

Aircraft mass and balance describes how the mass of an aircraft is distributed and how this distribution affects its flight characteristics. The most important concept in mass and balance analysis is the center of gravity (CG), which represents the point where the total mass of the aircraft can be considered to act. If the aircraft were supported exactly at the CG, it would remain in equilibrium without rotating [1]. Correct CG positioning is essential, as improper mass distribution may lead to reduced stability or loss of controllability.

To determine the CG location, a reference datum is defined. The reference datum is an arbitrary vertical plane from which all horizontal distances are measured. It is typically selected by the manufacturer at a convenient location such as the nose or firewall of the aircraft [1]. The horizontal distance between the reference datum and the CG of a specific component is called the arm. Arms located aft of the datum are considered positive, while those forward of the datum are negative. Each aircraft component produces a moment, defined as the product of its mass and arm. The moment represents the tendency of the mass to rotate the aircraft about the datum [2].

The position of the aircraft CG is calculated by summing all moments and dividing by the total mass of the aircraft:

$$x_{cg} = \frac{\sum M_i x_i}{\sum M_i}. \quad (1)$$

The numerator represents the total moment, while the denominator is the total aircraft mass. The resulting CG location is commonly expressed either as a distance from the datum or as a percentage of the mean aerodynamic chord (MAC), which is particularly useful for stability analysis [3].

In practice, mass and balance calculations follow a systematic procedure. First, the mass of each aircraft component is identified, including the basic empty aircraft, fuel, payload, and equipment. Second, the corresponding arms are obtained from aircraft documentation. Third, moments are calculated for each component. Finally, total mass and total moment are computed, allowing the CG location to be determined using the formula above. The calculated CG is then checked against the allowable CG envelope specified for the aircraft [1].

The CG position has a direct influence on aircraft stability. A forward CG generally increases longitudinal stability but reduces control authority, particularly during takeoff and landing, as larger control surface deflections are required to generate sufficient pitching moment [4]. The aft CG reduces stability and may lead to excessive sensitivity to disturbances or control inputs. If the CG moves too far aft, the aircraft may become longitudinally unstable and difficult to recover from stalls [5]. Hence, if the CG is not taken into consideration it may adversely affect the stability and controlability of aircraft.

It is also useful to understand all masses of the aircraft clearly and what is take-off mass of civil airplane consists from according to EASA [7]:

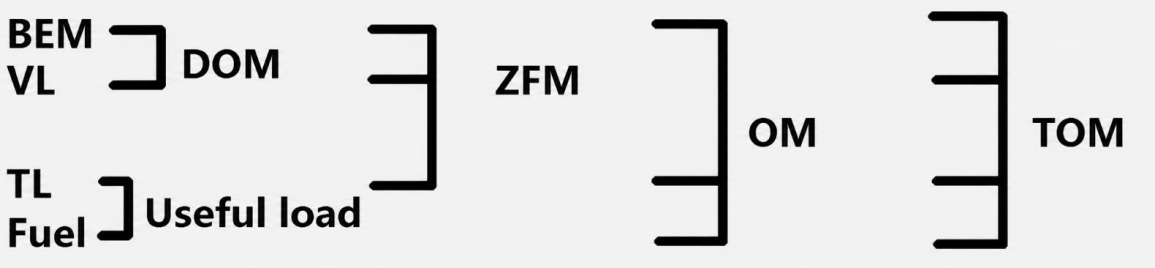

Fig. 1. Components of take-off mass

As it is seen BEM + VL = DOM, TL+ Fuel = Useful load, BEM + VL + TL = ZFM, BEM + TL + Fuel = OM and all components together give TOM. For light UAVs with military purposes sometimes VL= TL.

BEM is the mass of the unmanned aircraft (in our case) including the airframe, propulsion system, fixed onboard equipment and fixed energy source, excluding any payload.

VL is the mass that may change between missions and consists of the payload and any mission-dependent items.

TL is basically the same as payload and it is the mass of the mission equipment or cargo carried by the unmanned aircraft for the purpose of the flight.

Fuel refers to all fuel carried on board the aircraft. For an electrically powered UAV, this item is not applicable, since no fuel is carried on board and batteries are carried instead.

For the considered small UAV, the mass distribution is especially important because even relatively small payload shifts can noticeably change the CG position as a percentage of MAC. Therefore, the payload location is later used as the main variable for generating different CG cases. This allows the influence of forward, middle and aft CG positions on static and dynamic stability to be investigated without changing the external aerodynamic geometry of the aircraft.

In addition, for a light fixed-wing UAV the battery, payload module, avionics and propulsion system may represent a significant percentage of the total take-off mass. As a result, their longitudinal placement has a direct influence on the aircraft pitching behaviour. A forward shift of mass usually increases longitudinal static stability, but it may also require a larger elevator deflection to trim the aircraft. In contrast, an aft shift of mass reduces the static margin and may improve manoeuvrability, but it also decreases the natural tendency of the aircraft to return to equilibrium after a disturbance. For this reason, the mass and balance model used in this project is not only a weight accounting procedure, but also an important part of the stability analysis. By calculating the CG position for different payload locations, it becomes possible to define the safe operating range of the aircraft before performing aerodynamic and dynamic stability calculations.

2. Static Stability

Static stability refers to the initial response of an aircraft after it is subjected to a small disturbance from its equilibrium state. An aircraft is statically stable if the resulting aerodynamic forces and moments tend to restore the aircraft toward its original trimmed condition [3]. Static stability is evaluated independently in the longitudinal, lateral, and directional axes.

2.1. Longitudinal Static Stability

Longitudinal static stability concerns pitching motion. For an aircraft to be statically stable in pitch, an increase in angle of attack α must generate a restoring nose-down pitching moment. This condition is expressed using the pitching moment coefficient C_m. The aircraft is statically stable in pitch if the derivative of pitching moment coefficient with respect to angle of attack is negative:

$$C_{m_\alpha} = \frac{\partial C_m}{\partial \alpha} < 0. \tag{2}$$

A negative slope indicates that an increase in angle of attack produces a nose-down pitching moment, restoring equilibrium.

The main thing in longitudinal static stability is the neutral point. The neutral point is the CG position at which the aircraft exhibits neutral static stability, meaning that the pitching moment coefficient derivative with respect to angle of attack is zero. If the CG is located ahead of the neutral point, the aircraft is statically stable; if it is located aft of the neutral point, the aircraft becomes statically unstable [3].

The static margin is defined as the distance between the neutral point and the center of gravity, normalized by the mean aerodynamic chord:

$$SM = \frac{x_{np} - x_{cg}}{c_{MAC}}. \tag{3}$$

where x_{np} is the neutral point location, x_{cg} is the center of gravity position, and c_{MAC} is the mean aerodynamic chord. A positive static margin indicates stable flight. Typical aircraft operate with static margins between 5% and 15% of MAC, however UAV can be operated under higher SM of 20-25% [4]. Static Margin can be defined from C_m vs C_L curve, its slope coefficient and equation which will be shown further [17].

In this project, the static margin is one of the main parameters used to define the allowable CG envelope. A larger positive static margin provides stronger longitudinal restoring tendency after an angle-of-attack disturbance. However, an excessively large static margin may reduce pitch controllability and increase the elevator deflection required for trimming. For this reason, the selected CG range must provide a compromise between sufficient longitudinal stability and acceptable controllability.

2.2. Lateral Static Stability

Lateral static stability describes the aircraft's tendency to return to wings-level flight following a roll disturbance. This behaviour is mainly influenced by wing dihedral, wing placement, and sweep angle. The relevant stability derivative is the rolling moment coefficient with respect to sideslip angle:

$$C_{l_\beta} < 0. \tag{4}$$

A negative value indicates that a sideslip produces a restoring rolling moment. Wing dihedral is the primary contributor to this effect, as it causes the lower wing to generate more lift during a sideslip, rolling the aircraft back toward level flight.

2.3. Directional Static Stability

Directional static stability refers to yawing motion. An aircraft is directionally stable if it naturally aligns itself with the relative wind after a yaw disturbance. The vertical tail is the main contributor to directional stability. The stability condition is [3]:

$$C_{n_\beta} > 0. \tag{5}$$

A positive yawing moment coefficient derivative ensures a restoring yawing moment that realigns the aircraft with the airflow. Adequate directional stability is essential for coordinated flight and lateral-directional dynamic behaviour.

3. Dynamic Stability

Dynamic stability describes how an aircraft behaves over time following a disturbance. While static stability determines the initial tendency, dynamic stability determines whether the resulting motion decays, remains constant, or diverges [4]. Dynamic stability is analysed using linearised equations of motion about a trimmed flight condition.

The equations of motion are linearised assuming small perturbations and are typically separated into longitudinal and lateral-directional systems [6]. The dynamic response is characterised by eigenvalues of the system matrix. Stability requires that all eigenvalues have negative real parts[34].

3.1. Longitudinal Dynamic Modes

The longitudinal dynamics include two primary modes: the short-period mode and the phugoid mode.

The short-period mode is a fast, heavily damped oscillation involving angle of attack and pitch rate. It is primarily influenced by pitching moment derivatives such as C_{m_α} and C_{m_q}. A simplified representation of the short-period mode is:

$$\ddot{\alpha} + 2\zeta_{sp}\omega_{sp}\dot{\alpha} + \omega_{sp}^2\alpha = 0, \tag{6}$$

where ω_{sp} is the natural frequency and ζ_{sp} is the damping ratio [4]. A well-damped short-period mode ensures quick recovery from pitch disturbances. The phugoid mode is a slow oscillation involving exchange between kinetic and potential energy. It is characterised by variations in airspeed and altitude with a nearly constant angle of attack. Phugoid damping is typically weak and depends largely on drag characteristics [3].

3.2. Lateral-Directional Dynamic Modes

The lateral-directional dynamics include the Dutch roll, spiral, and roll subsidence modes. These modes describe the aircraft response to disturbances in yaw, roll, and sideslip, and they are important for evaluating lateral-directional stability. The Dutch roll is an oscillatory yaw-roll motion influenced by directional stability ($C_{n\beta}$) and dihedral effect ($C_{n\beta}$). Adequate damping is required to prevent undesirable yaw-roll oscillations, and yaw dampers or autopilot stabilization are often used to enhance Dutch roll damping [4]. The spiral mode is a slow, non-oscillatory mode that may be stable or unstable. A slight spiral instability is common and acceptable, as it usually develops slowly and can be corrected by pilot input or autopilot action [3]. The roll subsidence mode is a heavily damped, non-oscillatory mode that describes how quickly the roll rate decays after a roll disturbance or after control input removal. It is dominated by the roll damping derivative (C_{lp}) and is generally not a critical stability problem for conventional fixed-wing aircraft.

4. Types of Motions Following Disturbances

Types of motions following disturbances are shown on Fig. 2[25].

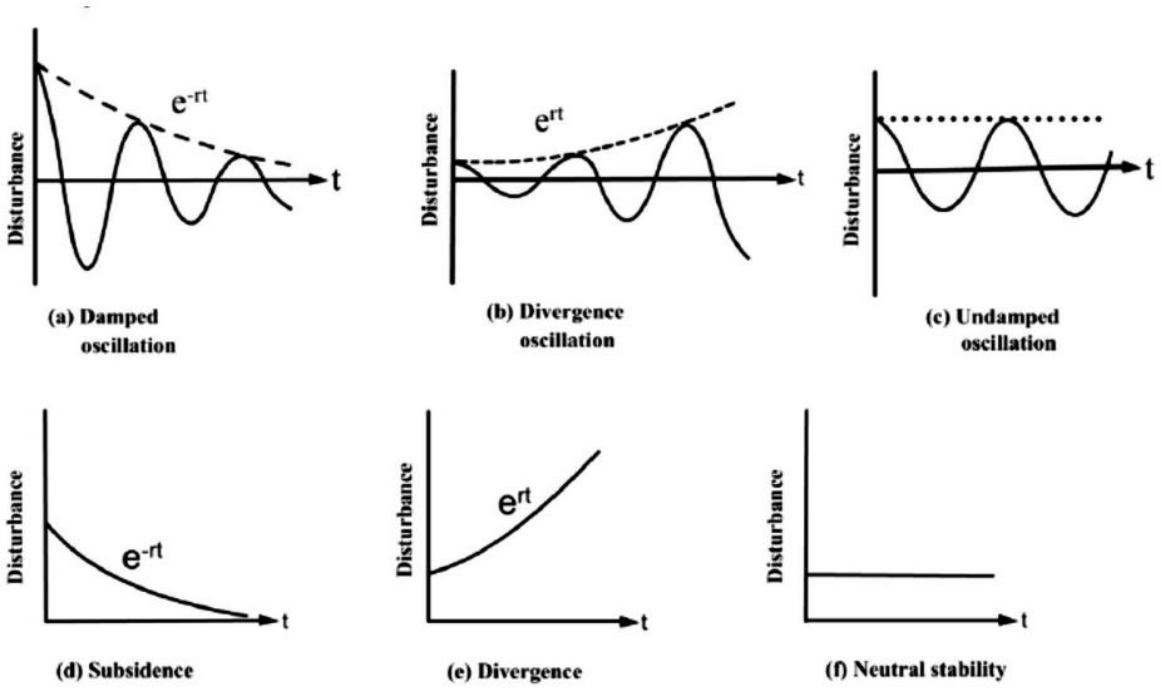

Fig. 2. Types of motions following disturbances

In a damped oscillation, the system oscillates around the equilibrium position, but the amplitude becomes smaller with time. Each oscillation is weaker than the previous one, and eventually the motion stops. The system finally returns to its equilibrium state

In an undamped oscillation, the system oscillates continuously with a constant amplitude. There is no loss of energy, so the motion never decreases and the system never settles at the equilibrium position

In subsidence, the system returns to the equilibrium position without oscillating. After being disturbed, it smoothly moves back to its original state and then stops.

In a divergent oscillation, the system oscillates, but the amplitude increases with time. Each oscillation becomes larger than the previous one, and the system moves farther away from equilibrium. This behaviour can eventually lead to instability or failure.

In divergence, the system moves away from the equilibrium position without oscillating. Once disturbed, it continuously departs from the equilibrium and never returns.

In neutral stability, the system remains in the disturbed position. After being displaced, it neither returns to equilibrium nor moves further away [25].

5. Software for Static and Dynamic Stability Analysis

Multiple programs can be used for static and dynamic stability analysis of light UAV. Among them most reasonable to look at seem XFLR5, AVL, OpenVSP with VSP Aero as well as Digital DATCOM.

5.1. XFLR5

XFLR5 is a free software package widely used for the aerodynamic and stability analysis of small aircraft operating at low speeds and low Reynolds numbers. It is especially popular in academic environments and UAV projects due to its graphical interface and relatively low learning curve. The software combines two-dimensional airfoil analysis with three-dimensional aerodynamic modeling based on lifting-line theory and the vortex lattice method. Two-dimensional airfoil characteristics are obtained using an internal XFOIL-based solver, while three-dimensional aerodynamic forces are computed for wings and tail surfaces [8][9][35].

In the context of stability analysis, XFLR5 is capable of estimating static and dynamic stability characteristics of a complete aircraft configuration. The software evaluates how aerodynamic forces and moments change when the aircraft experiences small variations in angle of attack, sideslip angle, angular rates, or control surface deflections. Based on these small perturbations, XFLR5 computes stability and control derivatives, which describe how sensitive the aircraft is to changes in attitude or control inputs [8].

A significant advantage of XFLR5 over many other preliminary tools is its built-in flight dynamics module. Using user-defined mass properties and center of gravity location, the software assembles a linearised flight dynamics model and identifies the main motion modes of the aircraft. These include longitudinal modes such as the short-period and phugoid motions, as well as lateral-directional modes such as Dutch roll, roll subsidence, and spiral motion. XFLR5 also provides a time-domain visualization of these modes, allowing the user to observe how the aircraft response evolves over a selected time interval following a small disturbance [9].

Center of gravity handling in XFLR5 is based on user input. The designer specifies the total mass, CG position, and approximate moments of inertia. These parameters are then used directly in stability and dynamic mode calculations. Although XFLR5 does not automatically compute CG from detailed internal geometry, this approach is sufficient for light UAVs, where CG is often obtained from a separate weight breakdown or simple CAD model. By varying the CG position manually, the user can investigate static margin and identify acceptable CG limits [10].

Despite its strengths, XFLR5 has limitations. The fuselage is either neglected or modeled in a simplified manner, and aerodynamic interactions such as propeller slipstream effects are not captured accurately. Additionally, the underlying aerodynamic methods are linear and inviscid, meaning that predictions become unreliable near stall or in strongly nonlinear regimes. Nevertheless, for early-stage design of conventional light UAVs, XFLR5 provides a balanced combination of usability, speed, and informative stability results [8][9]

5.2. FLOW5

FLOW5 is a free aerodynamic and stability analysis software which can be considered as an improved version of XFLR5. It is released by the same developer and developed to provide more stable numerical performance and more advanced tools for aircraft stability analysis while keeping a similar workflow and user interface.

Like XFLR5, FLOW5 uses two-dimensional airfoil data together with three-dimensional aerodynamic modeling based on the vortex lattice method. It is mainly intended for low-speed aircraft such as small UAVs and is suitable for preliminary design and stability evaluation.

In terms of stability analysis, FLOW5 computes aerodynamic stability and control derivatives based on small perturbations of flight conditions and control inputs. These derivatives are then used to analyze aircraft behaviour and stability characteristics.

The main difference between XFLR5 and FLOW5 is that while XFLR5 provides time-domain simulation of aircraft response, FLOW5 focuses on eigenvalue-based analysis, allowing direct assessment of damping, natural frequencies, and stability of motion modes such as short-period, phugoid, Dutch roll, spiral, and roll subsidence which is more consistent with classical flight dynamics methods [19].

5.3. AVL (Athena Vortex Lattice)

AVL is a computational tool developed for aerodynamic and flight dynamics analysis using an extended vortex lattice method. Unlike XFLR5, AVL is primarily operated through text-based input files, which describe the aircraft geometry, control surfaces, and analysis conditions. While this approach requires more discipline and experience, it offers a high level of flexibility and precision for users familiar with aircraft stability theory [11].

AVL models lifting surfaces using a vortex lattice representation and includes a simplified slender-body model for fuselages and nacelles. This allows the software to account for fuselage contributions to stability, particularly in yaw and pitching moments, which are often neglected in simpler wing-only models. Compressibility corrections can also be applied for moderate subsonic speeds, although AVL is most commonly used for low-speed applications relevant to UAVs [11].

In regards with stability analysis, AVL computes a complete set of aerodynamic stability and control derivatives. These derivatives describe how forces and moments change due to variations in angle of attack, sideslip angle, rotational motion, and control surface deflections such as elevator, aileron, and rudder inputs. The output can be expressed in different reference axes, allowing integration into flight dynamics models or control system simulations [11].

AVL has quite important thing such as its built-in linear flight dynamics analysis. When provided with aircraft mass, center of gravity, and inertia data, AVL constructs the linearised equations of motion and computes the characteristic motion modes of the aircraft. The software outputs eigenvalues and damping information for each mode, which allows direct assessment of dynamic

stability. This makes AVL particularly useful for verifying whether a UAV configuration exhibits acceptable dynamic behaviour before flight testing [11].

AVL does not compute mass properties automatically from geometry. Instead, the user defines component masses and their locations in a separate mass file. While this requires additional preparation, it allows precise control over CG placement and payload variation studies. For light UAVs, where mass distribution is often well known from component layouts, this approach is practical and effective.

Overall, AVL is a powerful and reliable tool for preliminary stability analysis. Its main disadvantages are the lack of a graphical interface and limited error feedback, which increase the risk of user-induced configuration mistakes. However, when used correctly, AVL provides high-quality stability predictions and is widely trusted in academic and industrial conceptual design studies [11].

5.4. OpenVSP with VSP Aero

OpenVSP is an open-source parametric aircraft geometry modeling environment developed by NASA. When combined with its aerodynamic solver VSP Aero, it forms a comprehensive toolset for conceptual aircraft design, including aerodynamic analysis, stability derivatives, and mass property estimation. Unlike XFLR5 and AVL, OpenVSP emphasizes full three-dimensional geometry representation of the entire aircraft, including fuselage, wings, and empennage [12][13].
VSP Aero performs aerodynamic analysis using inviscid potential flow methods, including vortex lattice and panel-based approaches. These methods allow OpenVSP to account for aerodynamic interactions between aircraft components, such as wing–fuselage and tail–fuselage interference. For light UAVs with non-negligible fuselage effects, this capability provides a more realistic representation of aircraft aerodynamics compared to wing-only models [13].

The stability analysis functionality in VSP Aero computes stability and control derivatives by applying small perturbations to the aircraft state or control surfaces. For example, the software can estimate how rolling or yawing moments change when ailerons or rudders are deflected, or how pitching moments vary with angle of attack. These derivatives are exported as numerical data, which can then be used for further flight dynamics analysis or control design [14].

Unlike XFLR5 and AVL, OpenVSP does not directly compute dynamic motion modes. Instead, it focuses on producing accurate aerodynamic derivatives and force coefficients. The dynamic analysis must therefore be completed in an external environment using the exported data and mass properties. One of OpenVSP's major strengths is its built-in mass properties analysis. The user can assign weights or material densities to individual aircraft components, and the software computes the total mass, center of gravity, and inertia tensor automatically. This feature makes OpenVSP particularly suitable for CG studies, payload placement analysis, and sensitivity studies related to mass distribution [13].

To sum up, OpenVSP with VSP Aero is well suited for early-stage UAV design where geometry, CG, and aerodynamic stability must be evaluated together. Its main drawback is the higher modeling effort and the lack of direct dynamic mode visualization. However, for configurations where fuselage effects are important, OpenVSP offers clear advantages over simpler tools [12][13].

5.5. Digital DATCOM

Digital DATCOM is a computer implementation of the United States Air Force Stability and Control DATCOM handbook. Unlike the previously mentioned tools, DATCOM does not solve aerodynamic flow equations. Instead, it uses a large collection of empirical and semi-empirical formulas derived from wind tunnel tests and theoretical studies of conventional aircraft configurations [15][16].

The software estimates aerodynamic coefficients and stability derivatives based on user-specified geometric parameters such as wing area, aspect ratio, tail volume, and fuselage dimensions. For classical wing with body and with tail configurations, DATCOM can provide reasonable estimates of static stability characteristics and control effectiveness with minimal computational effort [15].

DATCOM outputs a comprehensive set of stability derivatives, including those related to longitudinal, lateral, and directional stability, as well as control surface effectiveness. It also provides estimates of damping derivatives associated with rotational motion. However, the software does not perform dynamic mode analysis or time-domain simulation. Users who wish to analyze motion modes must export the results to a separate flight dynamics model [16].

Center of gravity handling in DATCOM is limited to specifying a reference point for moment calculations. The software does not compute CG or inertia values, and these must be obtained from external weight and balance calculations. As a result, DATCOM is typically used as a supporting or validation tool rather than a primary design environment.

Despite its age and limitations, Digital DATCOM remains valuable in academic settings as a benchmark and comparison tool. When used alongside modern vortex-lattice-based tools, it can help verify trends and identify potential inconsistencies in stability predictions for conventional UAV designs [15][16].

Table 1. Software for stability analysis comparison

Criteria	**XFLR5**	**FLOW5**	**AVL**	**OpenVSP + VSP Aero**	**Digital DATCOM**
Aerodynamic method	Vortex lattice / lifting-line with 2D airfoil data	Vortex lattice / lifting-line with 2D airfoil data	Extended vortex lattice with fuselage model	Vortex lattice / panel method on full 3D geometry	Empirical and semi-empirical formulas
Static stability derivatives	Yes	Yes	Yes	Yes	Yes
Dynamic motion modes	Yes (linear analysis with time response)	Yes (linear eigenvalue analysis)	Yes (eigenvalue analysis)	No	No
CG and inertia calculation	Manual input	Manual input	Manual input	Automatic from geometry	Not available
Fuselage influence	Limited	Limited	Approximate	Explicitly modeled	Empirical
User interface	Graphical (GUI)	Graphical (GUI)	Text-based	Graphical CAD-based	Text-based (GUI available)
Simulation	Yes	Yes	No	No	No

Suitability for light UAVs (MTOM < 10 kg)	**Very high**	**Very high**	**High**	**Very high**	**Moderate**

XFLR5, FLOW5 and OpenVSP with VSP Aero were found the most suitable for small UAV specifically for this project. Despite having a disadvantage of not precise fuselage calculation, XFLR5 and FLOW5 are the only softwares which have a simulation and show how the aircraft deviates and returns after disturbance at timeline (not just the graph and coefficients). Not precise fuselage calculation is considered to be acceptable for small UAV. FLOW5 is preferably to be used over XFLR5 as it has more consistent linear eigenvalue analysis for dynamic motion modes.

6. Methodology

The workflow of the project is organized as follows:
1. Definition of benchmark UAV requirements.
2. Geometrical sizing of the UAV.
3. Selection of airfoils and lifting surface geometry.
4. Component-based mass and balance modelling.
5. Definition of CG positions and design allowable CG envelope.
6. Calculation of neutral point and static margin.
7. Longitudinal static stability assessment.
8. Longitudinal and lateral-directional dynamic stability analysis.
9. Identification of weak stability modes and proposal of design improvements [20–24].

7. Benchmark Aircraft

A benchmark UAV will have the following requirements:

MTOM: 5 kg
Max wingspan: 2 m
V_s = 10 m/s = 36 km/h
V_c = 20 m/s = 72 km/h
V_{ne} = 35 m/s = 126 km/h

$C_{L(max)}$ taken is 1.25. The needed wing area can be identified by equation (7)[32].

$$S_{\text{req}} \geq \frac{2\,MTOM\,g}{\rho\, v_s^2\, C_{L,\max}}. \tag{7}$$

$$S_{req} \geq \frac{2 * 3 * 9.8}{1.225 * 8^2 * 1.25} \geq 0.64 \quad m^2$$

Horizontal tail volume coefficient equation can be seen below [28,29]:

$$V_{HTP} = \frac{l_{HTP} S_{HTP}}{\bar{c} S}. \tag{8}$$

Vertical tail volume coefficient equation can be found below:

$$V_{VTP} = \frac{l_{VTP}\, S_{VTP}}{b\, S}. \tag{9}$$

Having this in mind, recommended values in appendices 1 and 2, UAVs “Pirot Disco”, “AeroVironment Puma” , Cessna 150 and Cessna 172, the main geometrical properties of a benchmark are as following[33]:

Table 2. Main geometrical properties of the benchmark

Parameter	**Value**
Main wing span, b	2.00 m
Main wing area, S	0.64 m²
Main wing MAC, $\bar{c}$	0.32 m
Main wing aspect ratio, AR	6.25
Main wing taper ratio, λ	1.00
Main wing sweep, Λ	0°
Main wing aerodynamic centre, xAC,w	0.075 m
Horizontal tail span, b_{HTP}	0.60 m
Horizontal tail area, S_{HTP}	0.144 m²

Parameter	Value
Horizontal tail chord / MAC, c_{HTP}	0.24 m
Horizontal tail aspect ratio, AR_{HTP}	2.50
Horizontal tail aerodynamic centre, xAC_{HTP}	0.06 m
Vertical tail span / height, b_{VTP}	0.80 m
Vertical tail area, S_{VTP}	0.096 m²
Vertical tail chord / MAC, c_{VTP}	0.24 m
Vertical tail aspect ratio, AR_{VTP}	6.67
Vertical tail aerodynamic centre, xAC_{VTP}	0.06 m

For the main wing Eppler 399 airfoil was selected[17,39]:

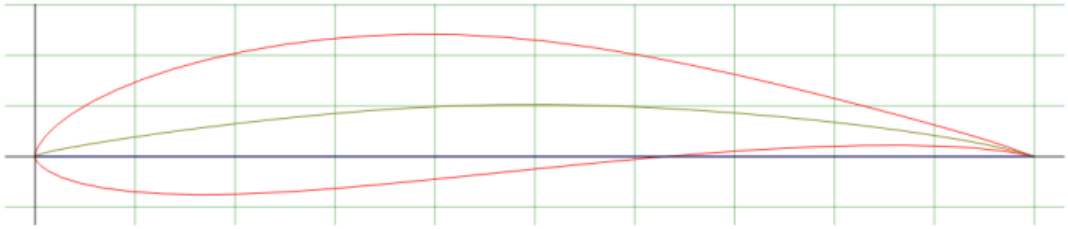

Fig. 3. Eppler 399 airfoil

The main properties of Eppler 399 are: Max thickness 14.8% at 29% chord. Max camber 5.1% at 51.4% chord.

For vertical and horizontal tailplane NACA 0009 symmetrical airfoil was selected with Max thickness 9% at 30.9% chord (camber is 0 as airfoil is symmetrical)[17,40]:

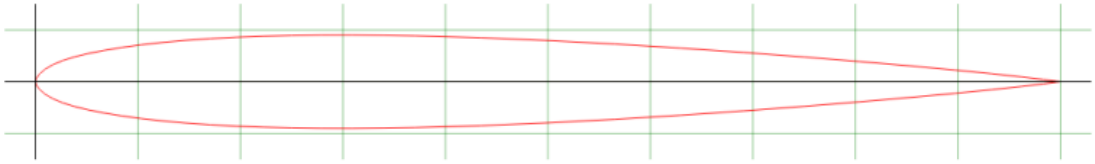

Fig. 4. NACA 0009 symmetrical airfoil

The geometry of the UAV (without fuselage) is built in FLOW5 and a sketch is made.

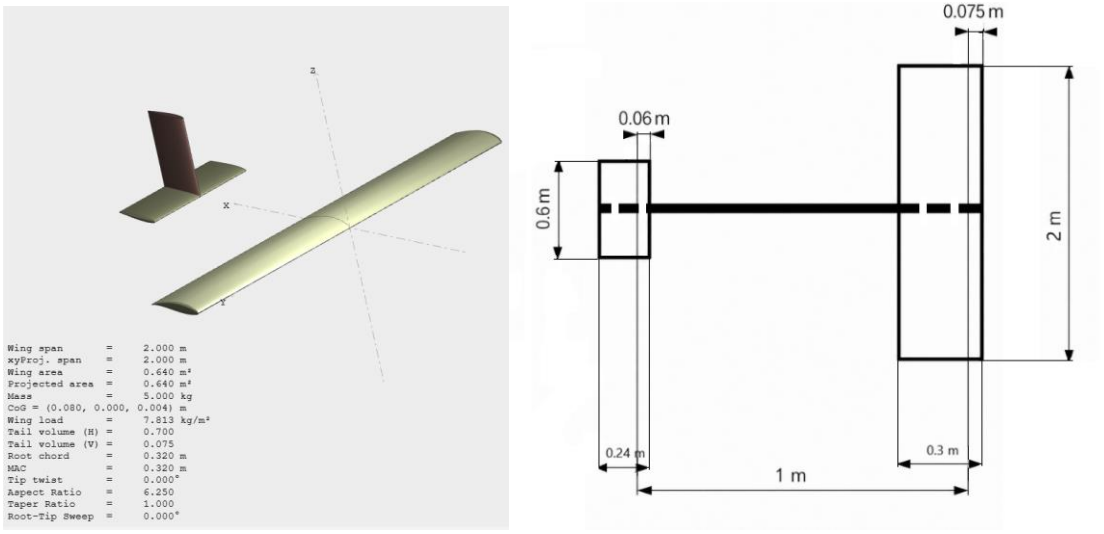

Fig. 5. UAV geometry built in FLOW5 and top sketch

The distance between the aerodynamic centre of the wing and the aerodynamic centre of the horizontal stabilizer is 1 m.

8. Stability Analysis in FLOW5

8.1. Mass and Balance

First of all, aircraft geometry is built. The masses should be distributed in order to obtain CG of about 25% MAC which will be used as a reference point for further calculations. Later on CG can be changed by shifting payload (TL) along the X-axis. For simplification all masses are distributed along the Y-axis symmetrically that is why all moment arms are 0. Datum is selected to be the leading edge of the main wing.

	Mass (kg)	x (m)	y (m)	z (m)	Description
1	1,000	0,050	0,000	0,000	Battery
2	1,000	-0,400	0,000	0,000	Engine and prop
3	2,000	0,157	0,000	0,000	Payload
4	0,100	1,150	0,000	0,200	Fin
5	0,150	1,150	0,000	0,000	Elevator
6	0,350	0,200	0,000	0,000	Wing
7	0,400	0,200	0,000	0,000	Fuselage

Fig. 6. Masses distribution along X-axis in FLOW5 at CG 25.1% MAC

After masses distribution the obtained CG is 25.1% MAC.

A VLM2+Drag (additional drag of fuselage with cross-sectional area of 0,02 m^2 was added) analysis was run at the following boundary conditions: ρ = 1,225 kg/m^3, v = 20 m/s, p = 1013.25 hPa. Standard meshing is used.
After analysis performance M_z vs C_L graph is obtained.

To calculate the neutral point, a graphical method is implemented using the line slope coefficient C_m vs C_L. The line is defined by two points but to reduce error 5 points were taken and the mean slope coefficient will be taken. The graph itself will be shown on Fig. 28.

For each adjacent pair, the local slope is:

$$m_{i,i+1} = \frac{\Delta C_m}{\Delta C_L} = \frac{C_{m,i+1} - C_{m,i}}{C_{L,i+1} - C_{L,i}}. \quad (10)$$

Point 1-2
$\Delta C_m = -0.06735 - (-0.07266) = +0.00531$
$\Delta C_L = 0.85950 - 0.88000 = -0.02050$
$m_{12} = 0.00531/(-0.02050) = \mathbf{-0.2590}$

Point 2-3
$\Delta C_m = -0.00349 - (-0.06735) = +0.06386$
$\Delta C_L = 0.61130 - 0.85950 = -0.24820$
$m_{23} = 0.06386/(-0.24820) = \mathbf{-0.2572}$

Point 3-4

$\Delta C_m = -0.00329 - (-0.00349) = +0.00020$
$\Delta C_L = 0.61050 - 0.61130 = -0.00080$
$m_{34} = 0.00020/(-0.00080) = \mathbf{-0.2500}$

Point 4-5
$\Delta C_m = -0.00308 - (-0.00329) = +0.00021$
$\Delta C_L = 0.60970 - 0.61050 = -0.00080$
$m_{45} = 0.00021/(-0.00080) = \mathbf{-0.2625}$

Mean local slope:

$\bar{m} \approx \mathbf{-0.2572}$

Now Neutral Point for CG 25.1% MAC can be calculated by using equation below:

$$\frac{x_{NP}}{c} = \frac{x_{CG}}{c} - \frac{dC_m}{dC_L}. \quad (11)$$

x_{NP} = 50.8 % MAC

Static Margin for CG 25.1% MAC can be calculated by using the following equation:

$$SM = \frac{x_{NP} - x_{CG}}{c} = \frac{x_{NP}}{c} - \frac{x_{CG}}{c}. \quad (12)$$

SM = 25.7% MAC

Static Margin is quite to the aft. Even though SM below 20% would be more preferable, still some small UAVs have SM in range between 20% and 25% [18,19,20]. Research on the conceptual design of small fixed-wing unmanned aerial systems, a static margin of approximately 20 % MAC is demonstrated as a design objective to ensure robust longitudinal stability [18,21].

So defined Static Margin for a benchmark is 20-25% MAC. An advantage of such an aft SM is that the aircraft is considered to be very stable however the controllability and maneuverability is expected to be weak [7].

Knowing SM limits, CG limits can be easily found below:

$$\frac{x_{CG}}{c} = \frac{x_{NP}}{c} - SM. \quad (13)$$

Rear CG limit can be found below:

$$\left(\frac{x_{CG}}{c}\right)_{aft} = 0.508 - 0.20 = 0.308$$

$x_{CG(aft)}$ = 30.8% MAC

Forward CG limit can be found below:

$$\left(\frac{x_{CG}}{c}\right)_{fwd} = 0.508 - 0.25 = 0.258$$

$x_{CG(fwd)}$ = 25.8% MAC

CG limit defined for benchmark UAV: **25.8-30.8% MAC**.

Now to investigate the stability of this aircraft three CGs were selected within the defined limits: aft limit, forward limit and CG in the middle between the limits.

$$CG_{mid} = \frac{CG_{aft} + CG_{fwd}}{2} . \quad (14)$$

CG_{mid} = 28.3 % MAC

To get the needed CGs all needed to do is to shift payload to aft or forward from datum.

Payload locations at each CG position are shown on Table 3.

Table 3. Payload locations at each CG position

CG, %MAC	**Payload location, m (aft from datum)**
25.8	0.163
28.3	0.181
30.8	0.203

8.2. Preliminary Stability Analysis

First, it is necessary to approximately identify the critical angle of attack AOA_{crit}. To do this, it is better to use the LLT (Lifting-Line Theory by Prandtl) method, as VLM2 (Vortex-Lattice Method 2) only calculates the linear relationship between the C_L and the Angle of Attack (*AOA*). *AOA* range selected: from -10 till 20.

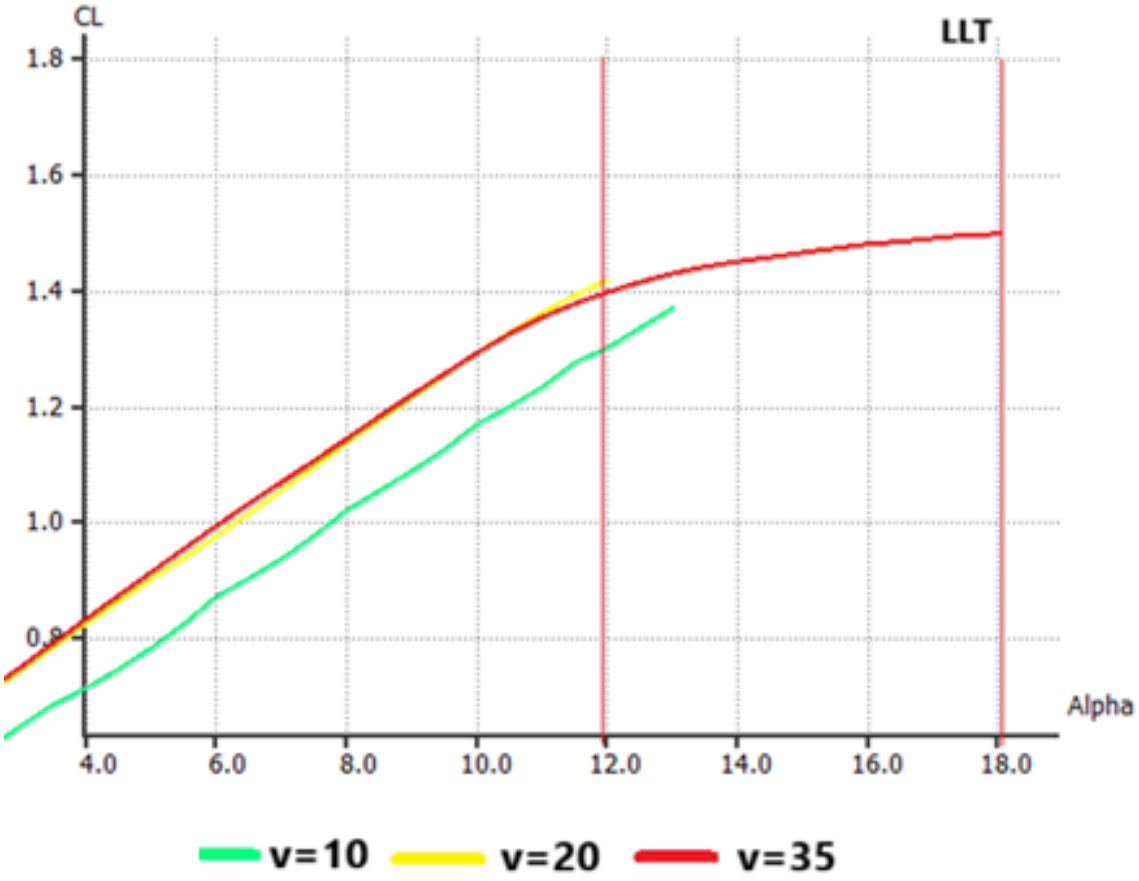

Fig. 7. C_L vs *AOA* by LLT method

From Fig. 7 it can be said that AOA_{crit} is 12˚ as LLT cannot find a solution for velocity of 20 m/s after *AOA* 12˚.

For all velocities (10, 20 and 35) and all CGs (25.8 %MAC, 28.3 %MAC, 30.8 %MAC) VLM2 analyses are performed under fixed speed for each case. The boundary conditions are ISA at elevation of 0.

C_m vs *AOA* curves are plotted and can be found below.

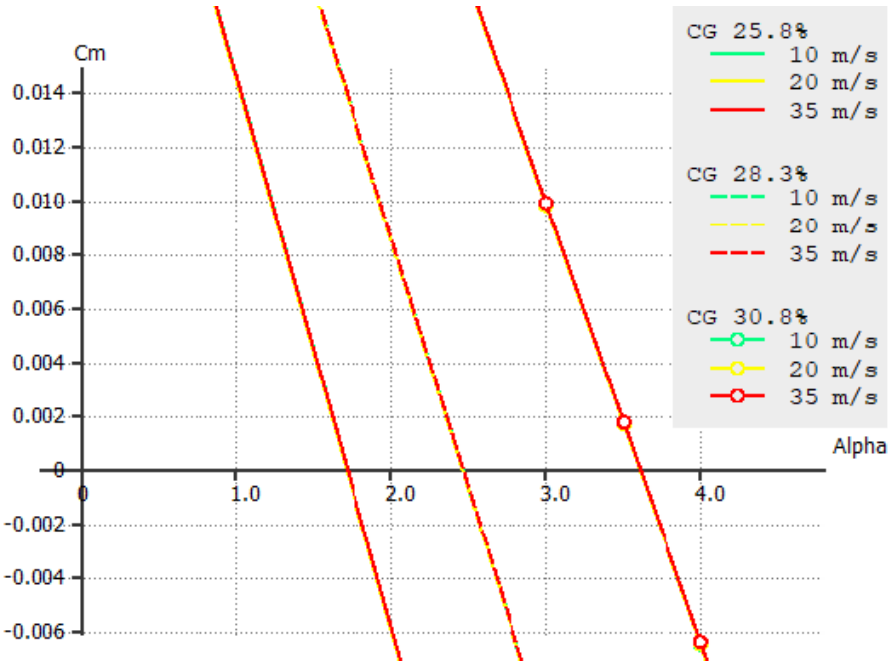

Fig. 8. C_m vs *AOA* for all CG configurations

From Fig. 7 it is seen that in all 3 CG options the lines are having nearly the same angle of slope which is reasonable for linear behaviour of wing and stabilizer at *AOA* from -0 till 4. The most important on this graph is C_{m0} (*AOA* at which $C_m = 0$). The lowest values of *AOA* with $C_m = 0$ are noticed at CG = 25.8%, AOA varies from 1.707 at v = 20 m/s till 1.714 at v = 10 m/s to be trimmed for the aircraft at this CG. For CG = 28.3% it is seen that trimmed *AOA* increases – at v = 20 m/s *AOA* of 2.45 is obtained and at v = 35 m/s *AOA* of 2.46 is obtained. At CG of 30.8% the aircraft is being trimmed from *AOA* of 1.19 till *AOA* of 1.21. The static longitudinal stability is not much influenced by changing the velocity.

Zoomed out C_m vs *AOA* curves are shown on Fig. 8.

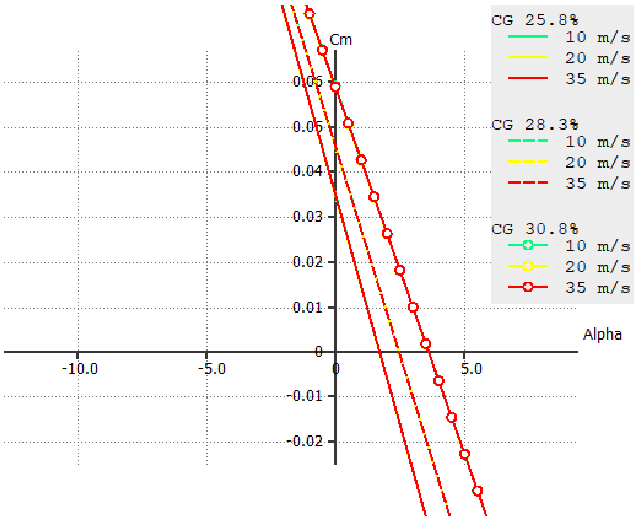

Fig. 9. C_m vs *AOA* for all CG configurations for *AOA* from -10° till +10°

From Fig. 8 it is seen that the aircraft is being longitudinally statically stable in *AOA* range from -10 to +10 as $\frac{dCm}{d\alpha} < 0$.

8.3. Longitudinal Stability

FLOW5 provides 4 modes of longitudinal stability. Modes 1 and 2 – short period. Modes 3 and 4 – phugoid.

Longitudinal stability is calculated in FLOW5 with control parameter from 0 till 1 and delta t of 0.1 second.

Modes 1 and 2 for CG 25.8% MAC can be seen below.

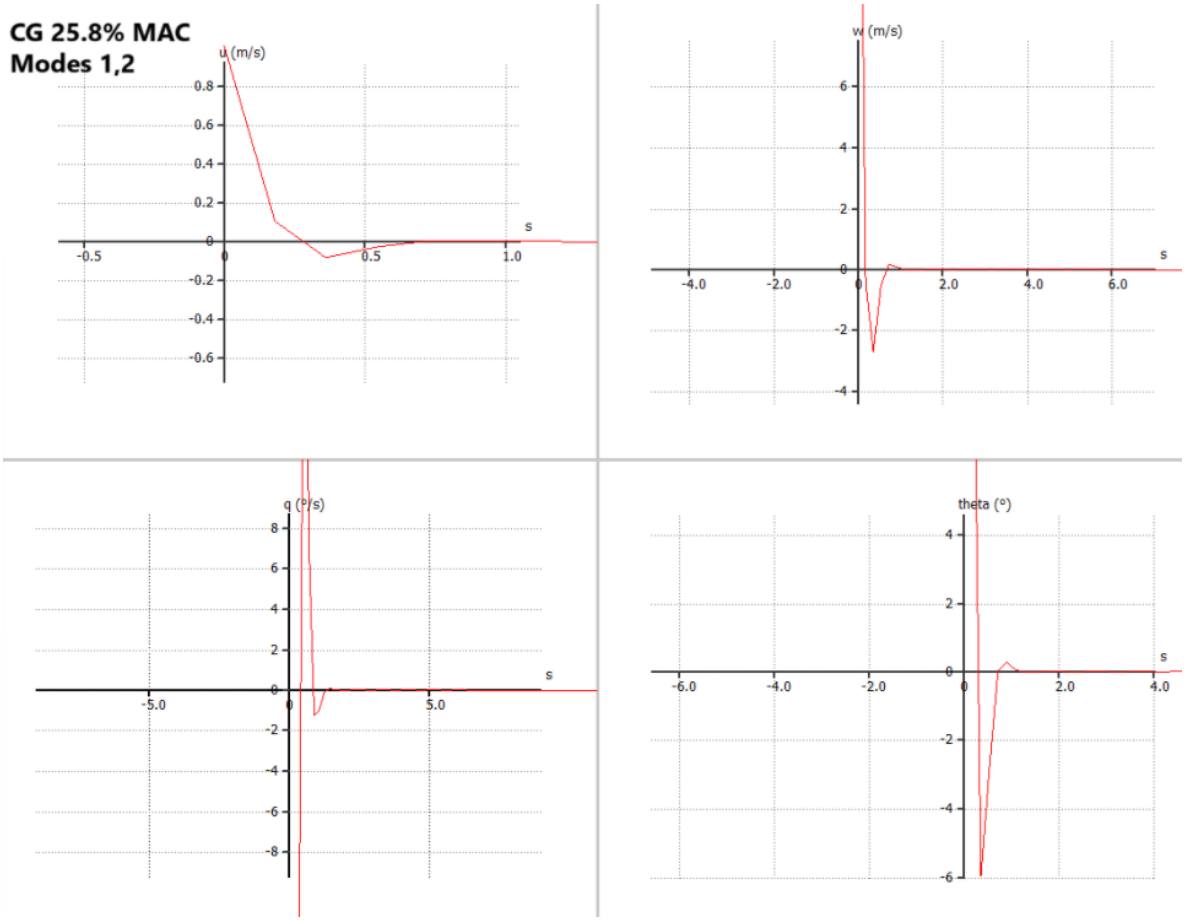

Fig. 10. Modes 1,2 for CG 25.8% MAC, longitudinal

From Fig. 7 it is seen that oscillations dampen very fast. Aircraft returns to equilibrium within less than 2 seconds.

The short-period mode is characterised by the eigenvalues $\lambda = -6.30 \pm 6.89i$, corresponding to a natural frequency of $f_n = 1.485$ Hz and a damping ratio of $\zeta = 0.68$. This indicates a fast and well-damped short-period response [26].

Modes 1 and 2 for CG 28.3% MAC can be seen below.

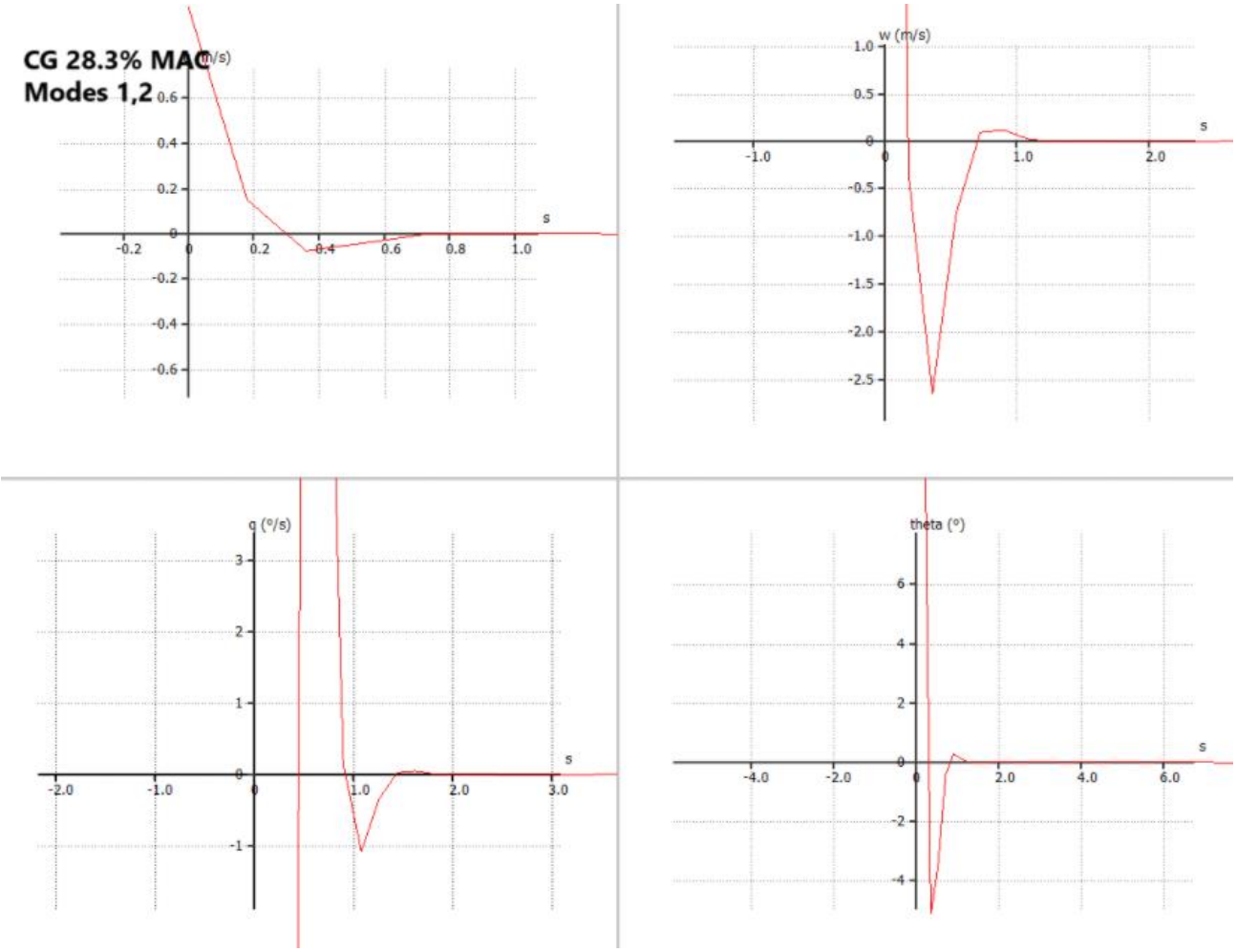

Fig. 11. Modes 1,2 for CG 28.3% MAC, longitudinal

From Fig. 8 it is understandable that for "middle" CG of 28.3 % MAC at modes 1 and 2 the aircraft returns to the equilibrium very fast and does it within less than 2 seconds.

It can be said that at this CG the short-period mode remains stable with eigenvalues $\lambda \approx -5.899 \pm 6.245i$, natural frequency $f_n = 1.367$ Hz, and damping ratio $\zeta = 0.687$. Compared to the more forward CG case (25.8% MAC), the natural frequency decreases slightly, indicating a slower short-period response, while the damping ratio increases marginally, indicating slightly improved damping. Overall, the changes are nearly unnoticeable.

Modes 1 and 2 for CG 30.8% MAC are represented below on Fig. 12.

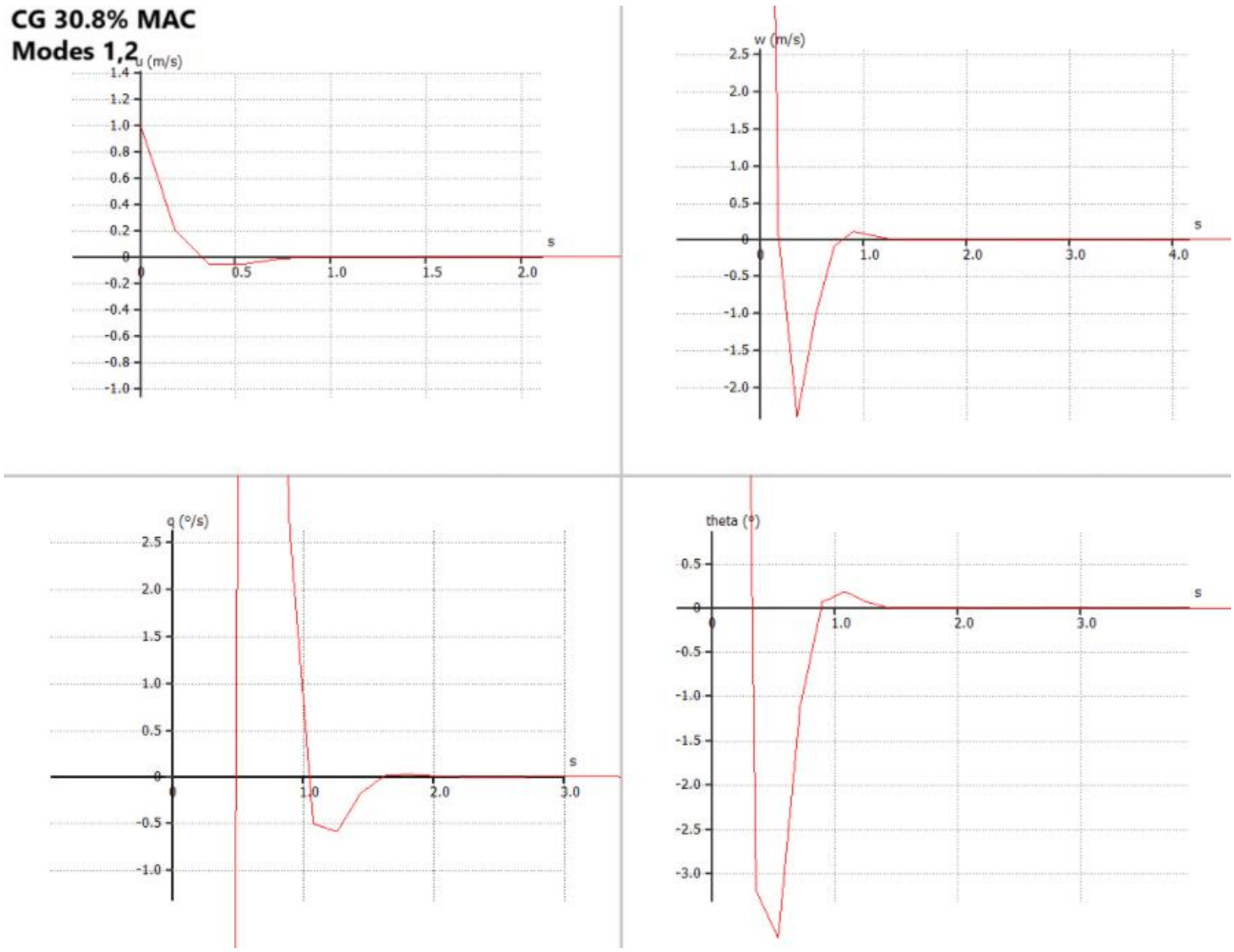

Fig. 12. Modes 1,2 for CG 30.8% MAC, longitudinal

At CG = 30.8% MAC the short-period mode is characterised by the eigenvalues $\lambda = -5.41 \pm 5.46i$, a natural frequency of $f_n = 1.223$ Hz, and a damping ratio of $\zeta = 0.703$. Compared to more forward CG positions, the short-period natural frequency decreases, indicating a less stiff pitch response, while the damping ratio increases, resulting in a well-damped and stable short-period motion.

In general, the modes 1 and 2 for all CGs are perfect with very fast damping less than 2 seconds till complete equilibrium.

Modes 3 and 4 for CG of 25.8 % MAC are shown below.

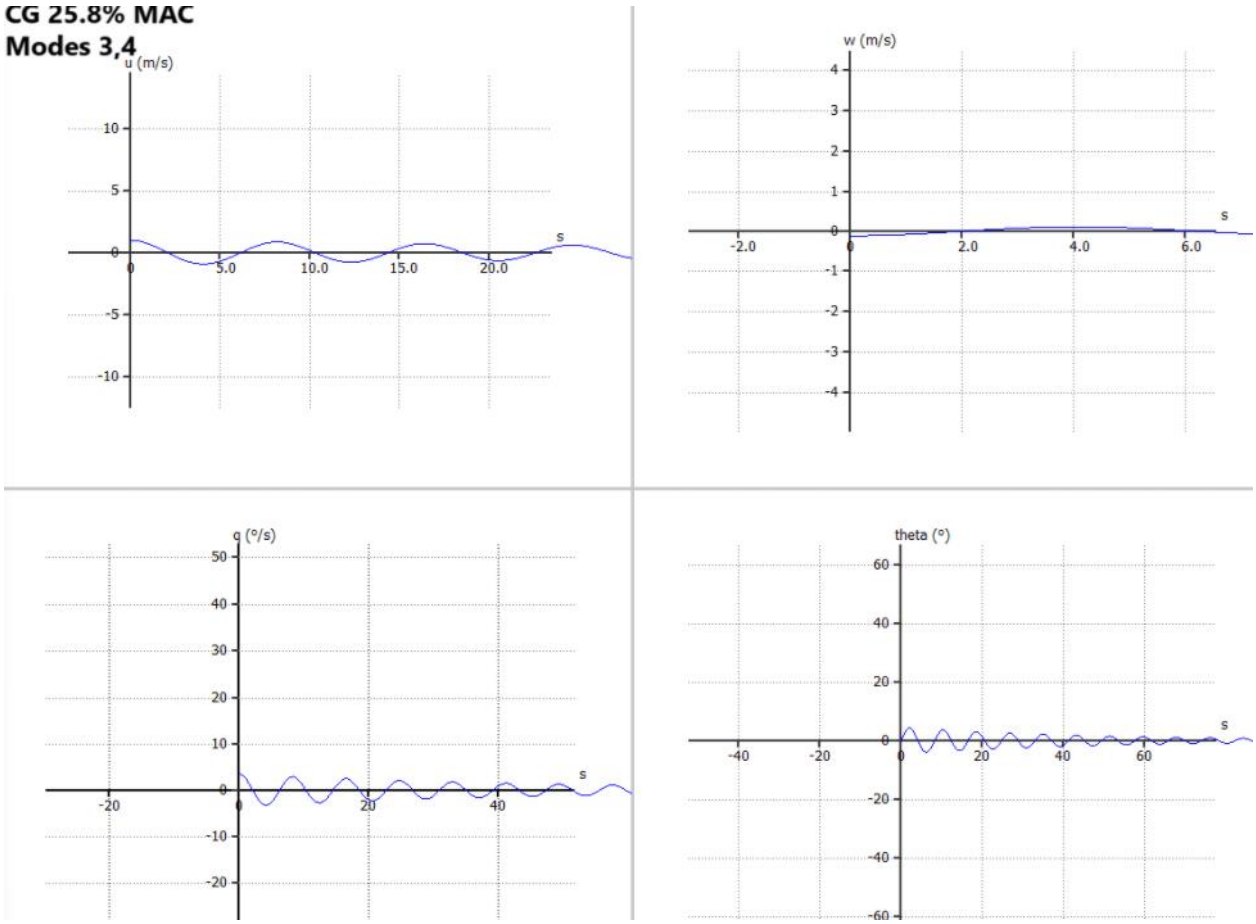

Fig. 13 Modes 3,4 for CG 25.8% MAC, longitudinal

Even though aircraft shows longitudinal stability at modes 3 and 4 as oscillations dampen, they dampen at a very slow manner. Judging by the curves, Pitch rate q and pitch angle theta are being damped to approximately 10% at more than 90 seconds

Phugoid mode here is characterised by the eigenvalues $\lambda = -0.025 \pm 0.766i$, corresponding to a natural frequency of $f_n = 0.122$ Hz and a damping ratio of $\zeta = 0.027$. This indicates a lightly damped, long-period longitudinal oscillation, which is typical for small UAVs [26].

The precise time after which the aircraft approaches the equilibrium having oscillation damped to 10% can be found using equation below [26]:

$$t_p = \frac{\ln(1/p)}{-\sigma}. \tag{15}$$

$t_{p,CG25.8}$ = ln10/0.025 = **92 sec**

Modes 3 and 4 for “medium” CG of 28.3% are represented below.

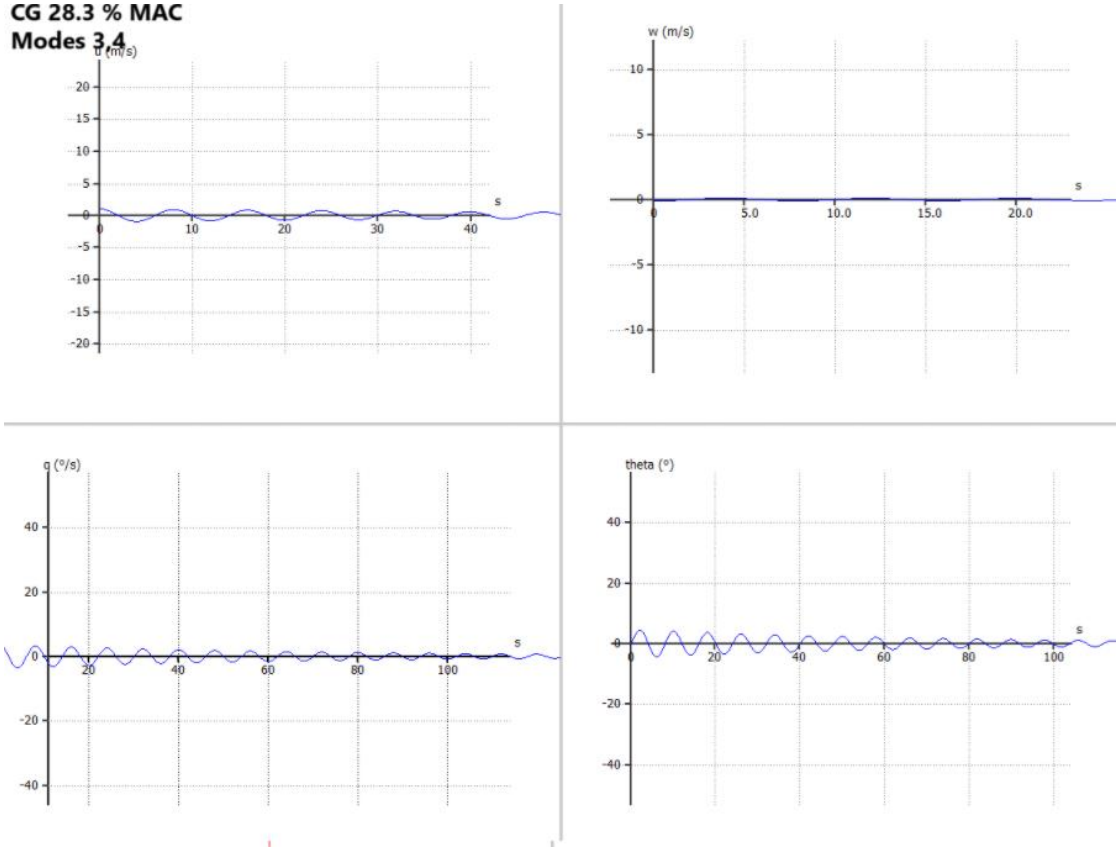

Fig. 14. Modes 3,4 for CG 28.3% MAC, longitudinal

At CG = 28.3% MAC, the phugoid mode is characterised by the eigenvalues $\lambda = -0.0140 \pm 0.7883i$, a natural frequency of $f_n = 0.125$ Hz, and a damping ratio of $\zeta = 0.018$. The mode remains dynamically stable but is very lightly damped. Compared to the more forward CG position at 25.8% MAC where the natural frequency was $f_n = 0.122$ Hz and the oscillation amplitude damped to 10% within 92 seconds, the phugoid frequency remains almost the same while the damping deteriorates significantly. The time required for the oscillations to be damped to 10% of their initial amplitude is more than 120 seconds judging by the graphs.

To define when the oscillations are dampen to 10% the same formula as for the previous case is used:

$t_{p,CG28.3}$ = ln10/0.014 = **164.5 sec**

So the time for the oscillations to dampen to 10% increased by 1.8 times compared to the CG of 25.8% MAC.

Modes 3 and 4 for the most aft CG of 30.8% are represented on Fig. 12 below:

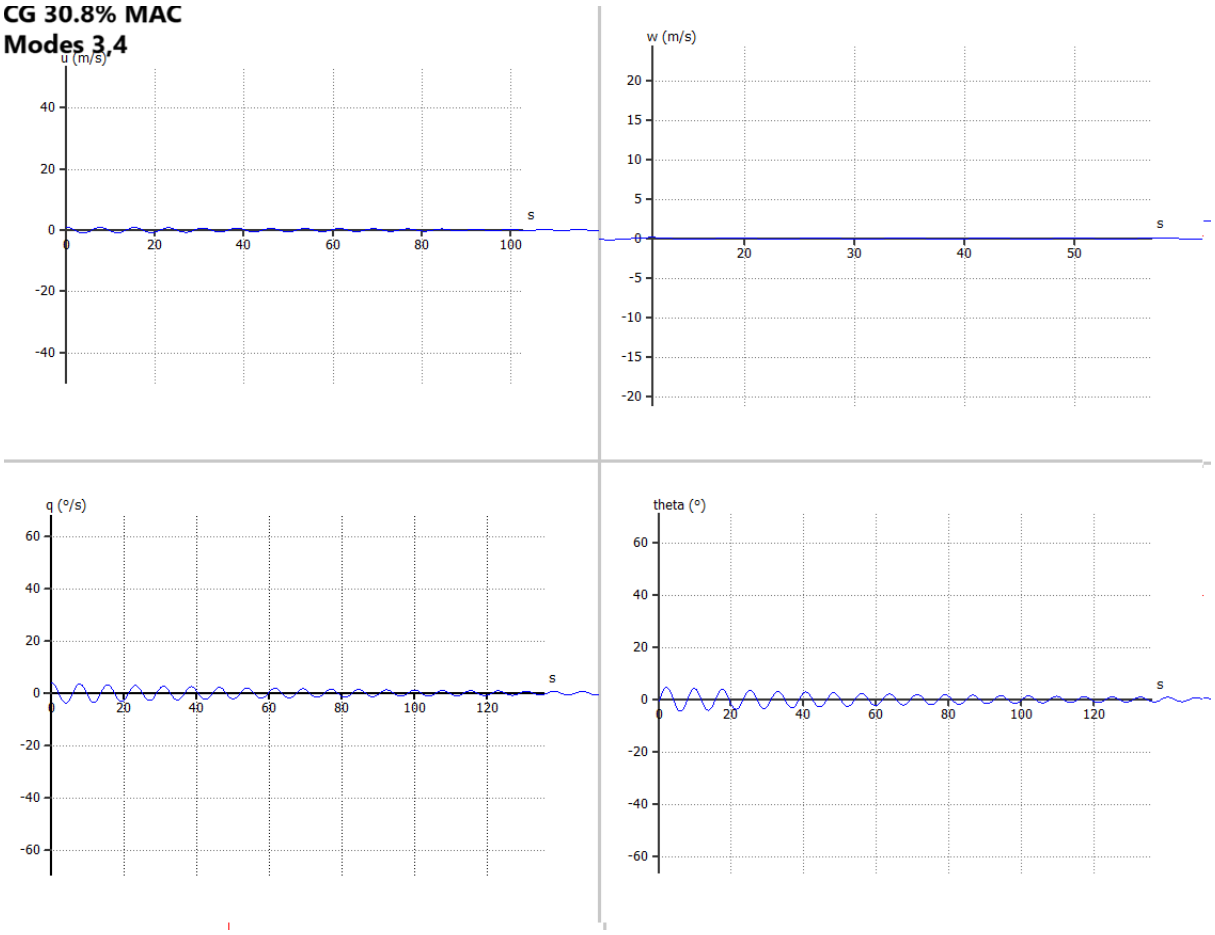

Fig. 15. Modes 3,4 for CG 30.8% MAC, longitudinal

For the most aft CG of 30.8% $\lambda = -0.0151 \pm 0.8192i$, $f_n = 0.130$ Hz, $\zeta = 0.0151$. The mode remains dynamically stable (negative real part), but it is very lightly damped. Judging by the real part of the eigenvalue of 0.0151 it can be easily predicted that damping time to 10% will slightly decrease.

$t_{p,CG30.8}$ = ln10/0.014 = **153 sec**

It can be said that in phugoid mode the aircraft is dynamically stable at all CGs. However, damping in this mode is very slow. The slowest is 164.5 sec at CG of 28.3% MAC. It should be taken into account especially if the UAV is planned to be flown manually without autopilot. It is recommended to install autopilot which will change pitch as a countermeasure to phugoid. However, generally for this kind of light UAV these values are acceptable. For example, a much bigger agricultural UAV (concept) with MTOM 280 kg shows eigenvalues $\lambda = -0.00527 \pm 0.53300i$ and damping ratio $\zeta = 0.00989$ [27].

8.4. Lateral-Directional Stability

FLOW5 provides 4 modes of lateral-directional stability. Mode 1 – roll damping (basically it is lateral stability mode). Modes 2 and 3 – Dutch Roll. Mode 4 – spiral.

Lateral-directional stability is calculated in FLOW5 with control parameter from 0 till 1 and delta t of 0.1 second.

Oscillations of Mode 1 for CG 25.8%, 28.3% and 30.8% MAC can be found below in figures 14, 15 and 16 respectively.

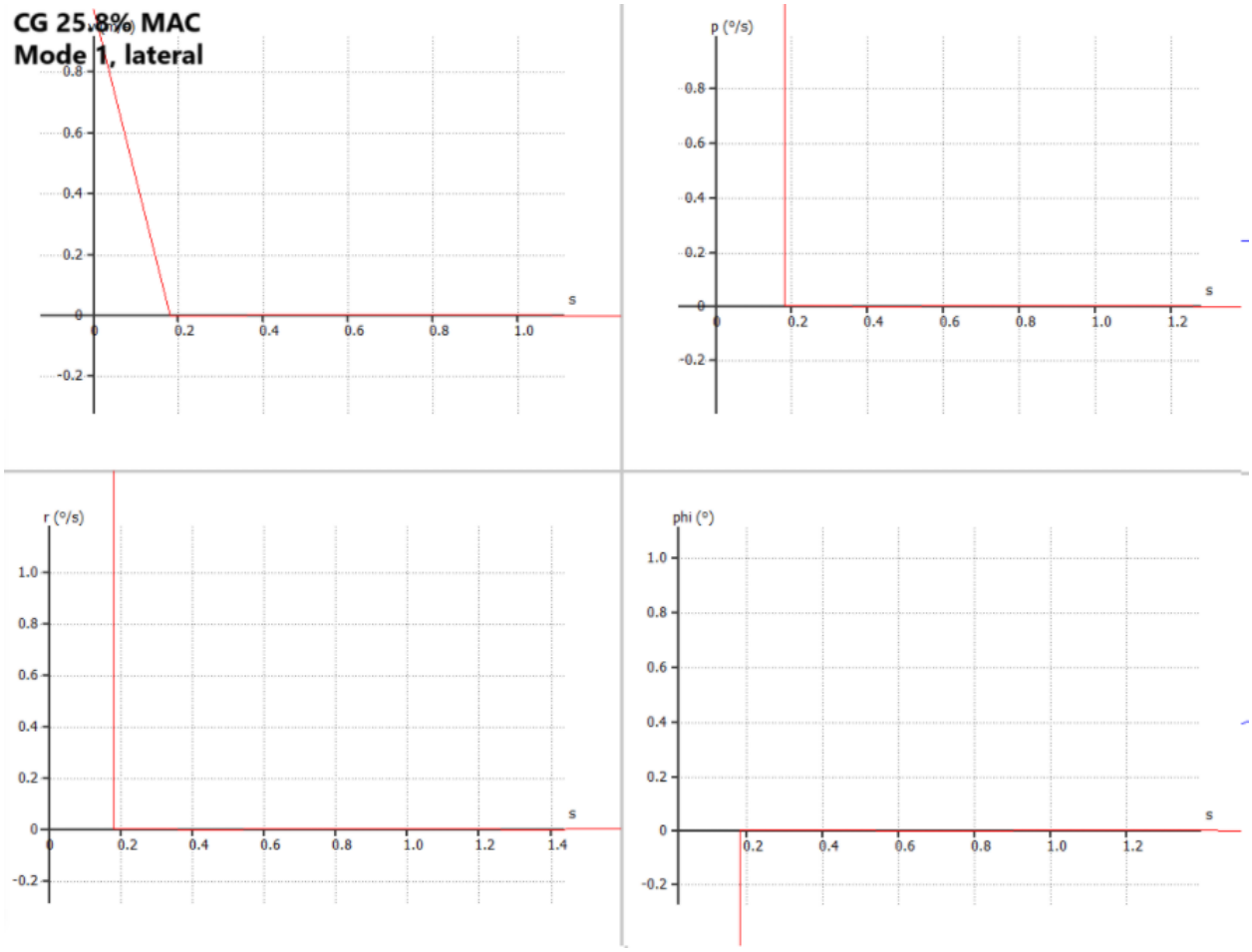

Fig. 16. Mode 1 for CG 25.8% MAC, lateral

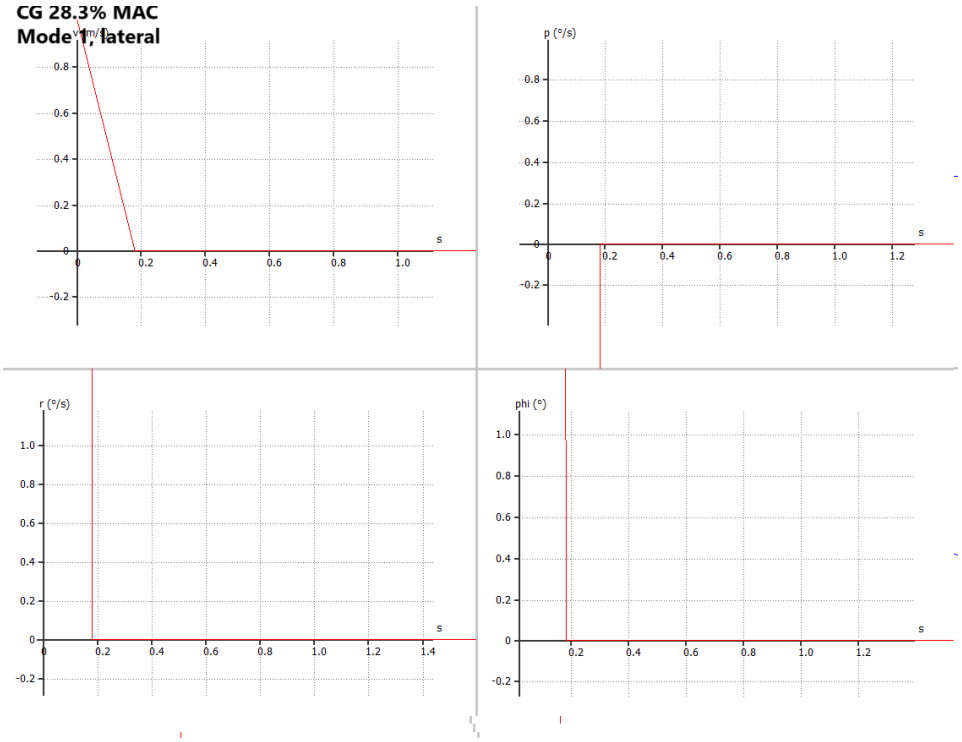

Fig. 17. Mode 1 for CG 28.3% MAC, lateral

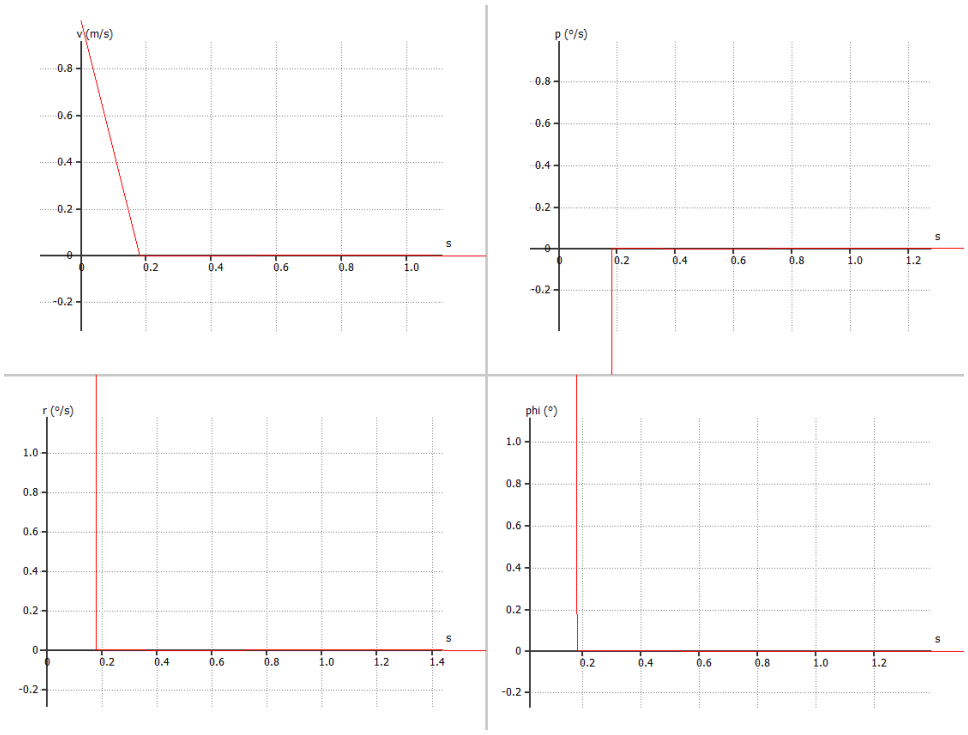

Fig. 18. Mode 1 for CG 30.8% MAC, lateral

From figures 14, 15 and 16 it is clearly seen that in roll damping mode UAV returns to the equilibrium less than within 0.2 sec which is a very good result. The UAV is dynamically stable in lateral mode 1.

Lateral-directional mode Dutch roll (or modes 2 and 3) for CG 25.8% MAC can be found below.

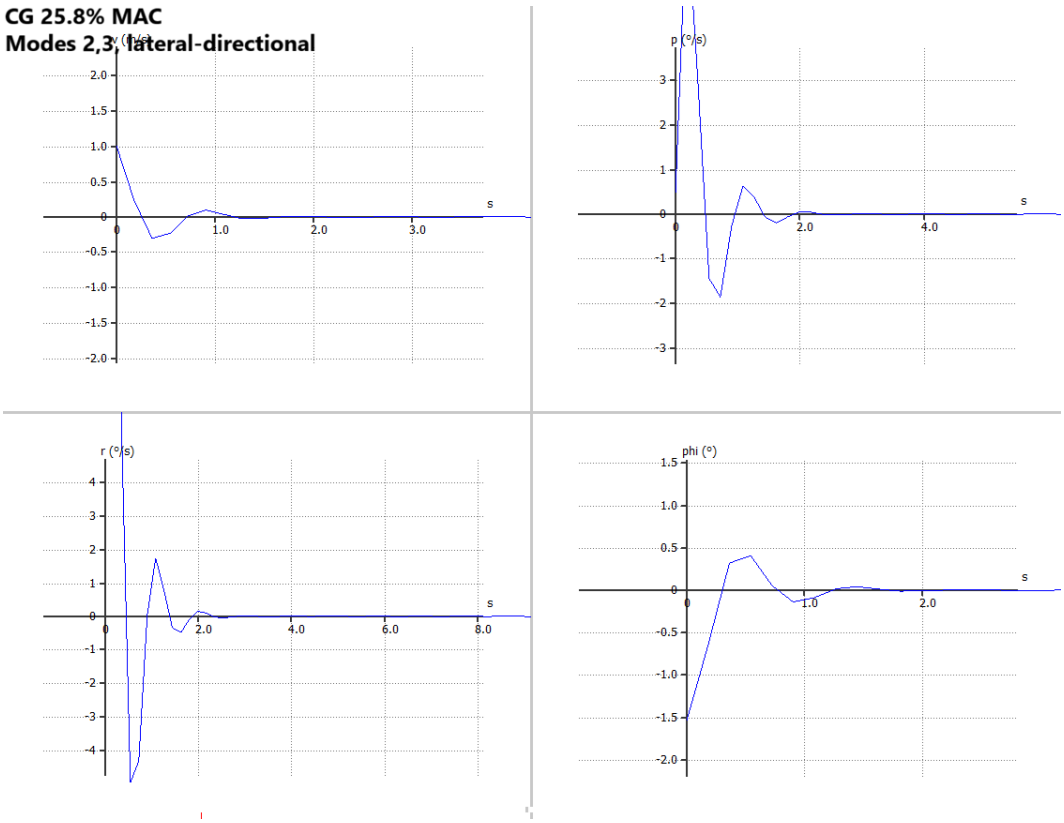

Fig. 19. Modes 2,3 for CG 25.8% MAC, lateral-directional

At CG = 25.8% MAC the Dutch roll mode (modes 2 and 3) is represented by the eigenvalues $\lambda = -2.252 \pm 6.684i$, corresponding to a natural frequency of $f_n = 1.137$ Hz and a damping ratio of $\zeta = 0.353$. The negative real part confirms that the mode is dynamically stable, while the imaginary part indicates an oscillatory response.

Time needed for the oscillations to dampen to 10% and 1% of amplitude is calculated below respectively:

$t_{dutch,25.8,10\%}$ = ln(10)/2.252 = **1.02 sec**
$t_{dutch,25.8,1\%}$ = ln(100)/2.252 = **2.04 sec**

The results are perfect as for the small UAV.

Dutch roll mode for CG 28.3% MAC is represented below.

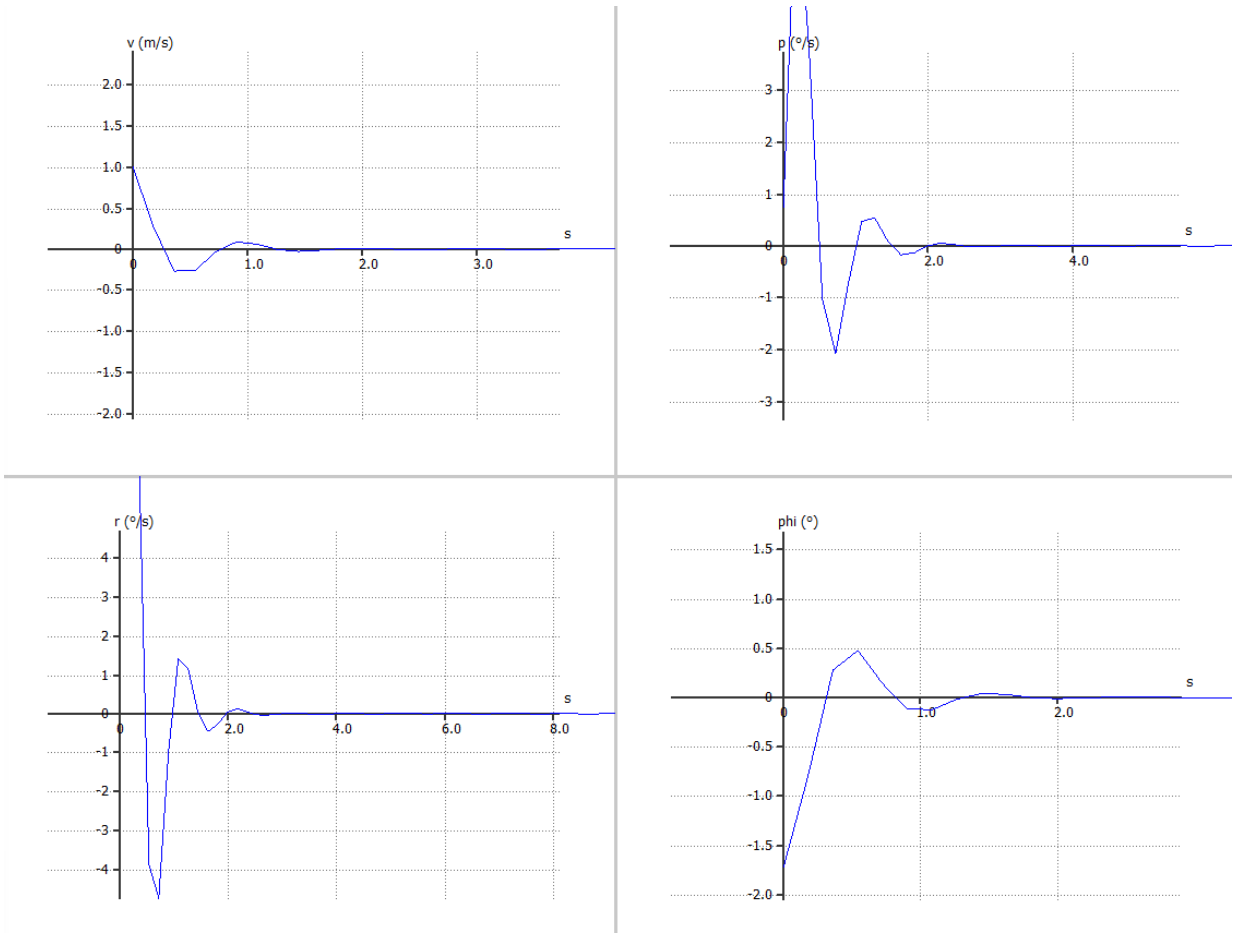

Fig. 20. Modes 2,3 for CG 28.3% MAC, lateral-directional

For CG 28.3% MAC, the aircraft also shows very good behaviour while recovering after the Dutch roll mode. Eigenvalues $\lambda = -2.467 \pm 6.307i$, with a natural frequency $f_n = 1.078$ Hzand a damping ratio $\zeta = 0.364$.

Time needed for the oscillations to dampen to 10% and 1% of amplitude is calculated below respectively:

$t_{dutch,28.3,10\%}$ = ln(10)/2.467 = **0.93 sec**
$t_{dutch,28.3,1\%}$ = ln(100)/2.467 = **1.87 sec**

Dutch roll mode for CG 30.8% MAC is shown below.

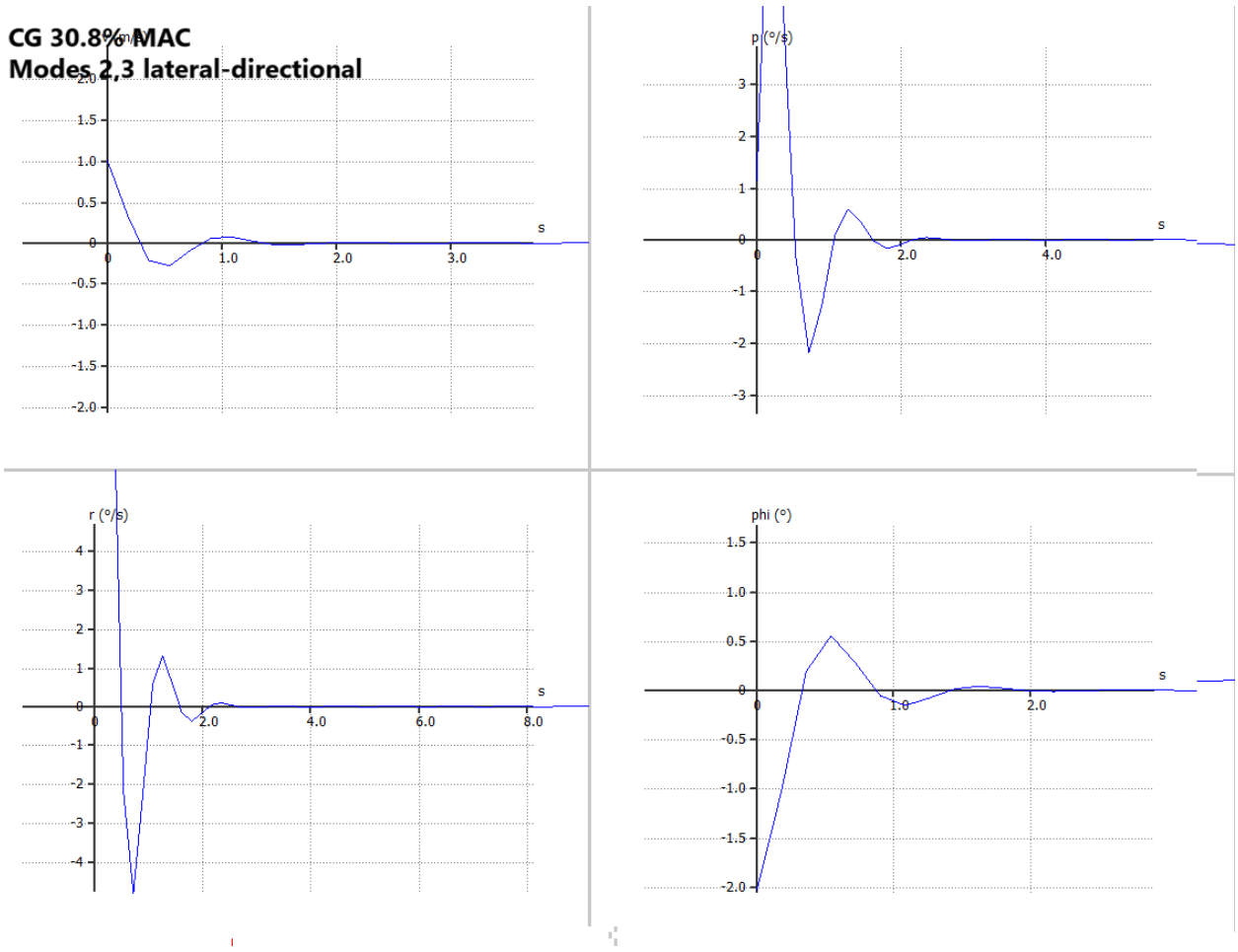

Fig. 21. Modes 2,3 for CG 30.8% MAC, lateral-directional

At CG 30.8% MAC the Dutch roll mode is represented by the eigenvalues $\lambda = -2.401 \pm 5.828i$, with a natural frequency $f_n = 1.003$ Hz and a damping ratio $\zeta = 0.381$.

Time needed for the oscillations to dampen to 10% and 1% of amplitude is calculated below respectively:

$t_{dutch,30.8,10\%}$ = ln(10)/2.401 = **0.96 sec**
$t_{dutch,30.8,1\%}$ = ln(100)/2.401 = **1.92 sec**

Across all investigated CG positions the Dutch roll mode of the UAV remains dynamically stable and very well damped. It can be said that less than 3 seconds are needed for the system to come to equilibrium.

Mode 4, also known as Spiral mode oscillations for CG 25.8% MAC are shown below.

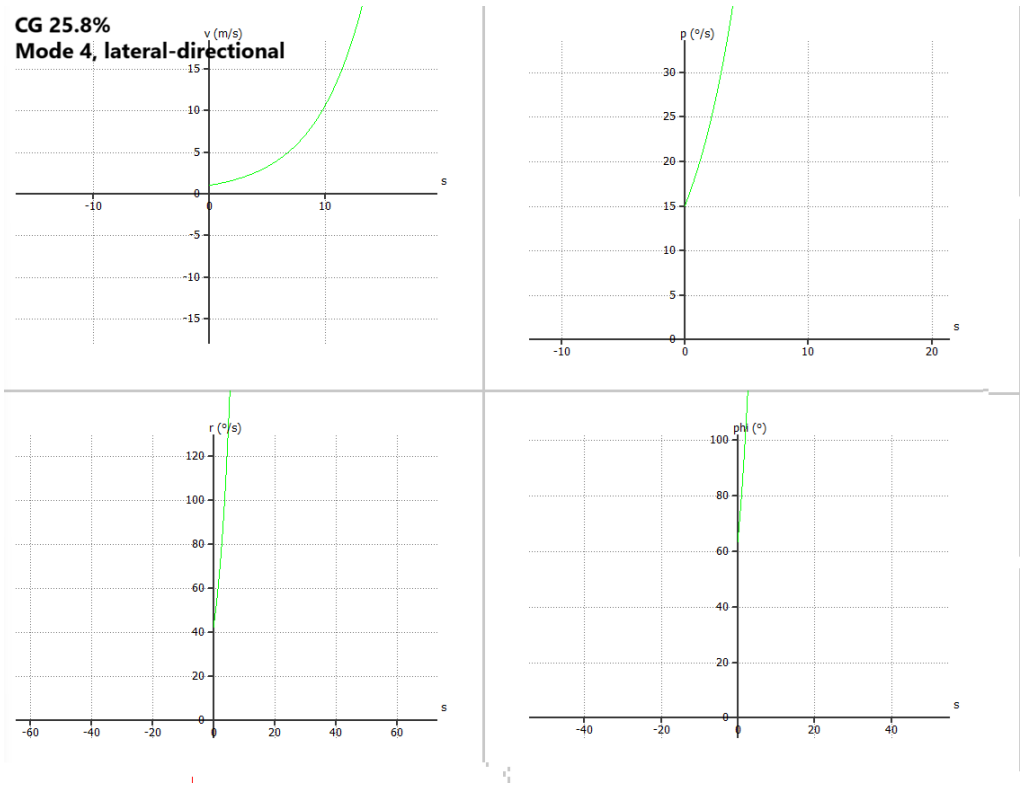

Fig. 22. Mode 4 for CG 25.8% MAC, lateral-directional

For CG 25.8% MAC, the spiral mode is represented by a small positive real eigenvalue $\lambda = +0.236$, indicating a weakly unstable aperiodic response. Having a divergence it is still crucial to understand after how fast amplitude increases twice and 10 times.

$t_{25.8,2x}$ = ln2/0.236 = **2.61 sec**
$t_{25.8,10x}$ = ln10/0.236 = **8.66 sec**

It means that amplitude of roll and yaw will increase slightly faster on "middle" CG if the flight controls are not touched.

Mode 4 for CG 28.3% MAC is shown below.

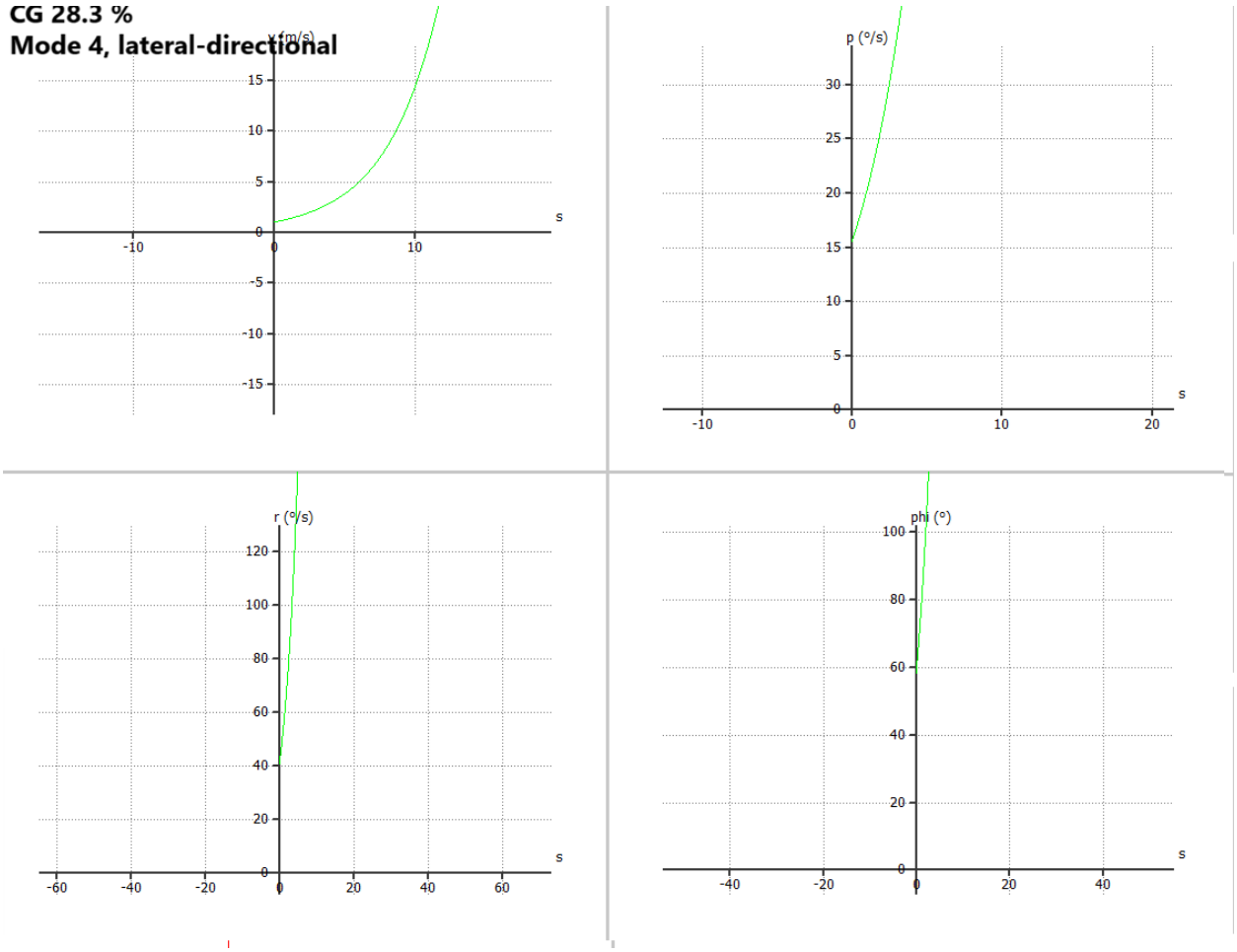

Fig. 23. Mode 4 for CG 28.3% MAC, lateral-directional

At CG 28.3% MAC, the spiral mode is represented by a purely real positive eigenvalue $\lambda = +0.266$, indicating a weakly unstable aperiodic spiral divergence.

$t_{28.3,2x}$ = ln2/0.266 = **2.94 sec**
$t_{28.3,10x}$ = ln10/0.266 = **9.75 sec**

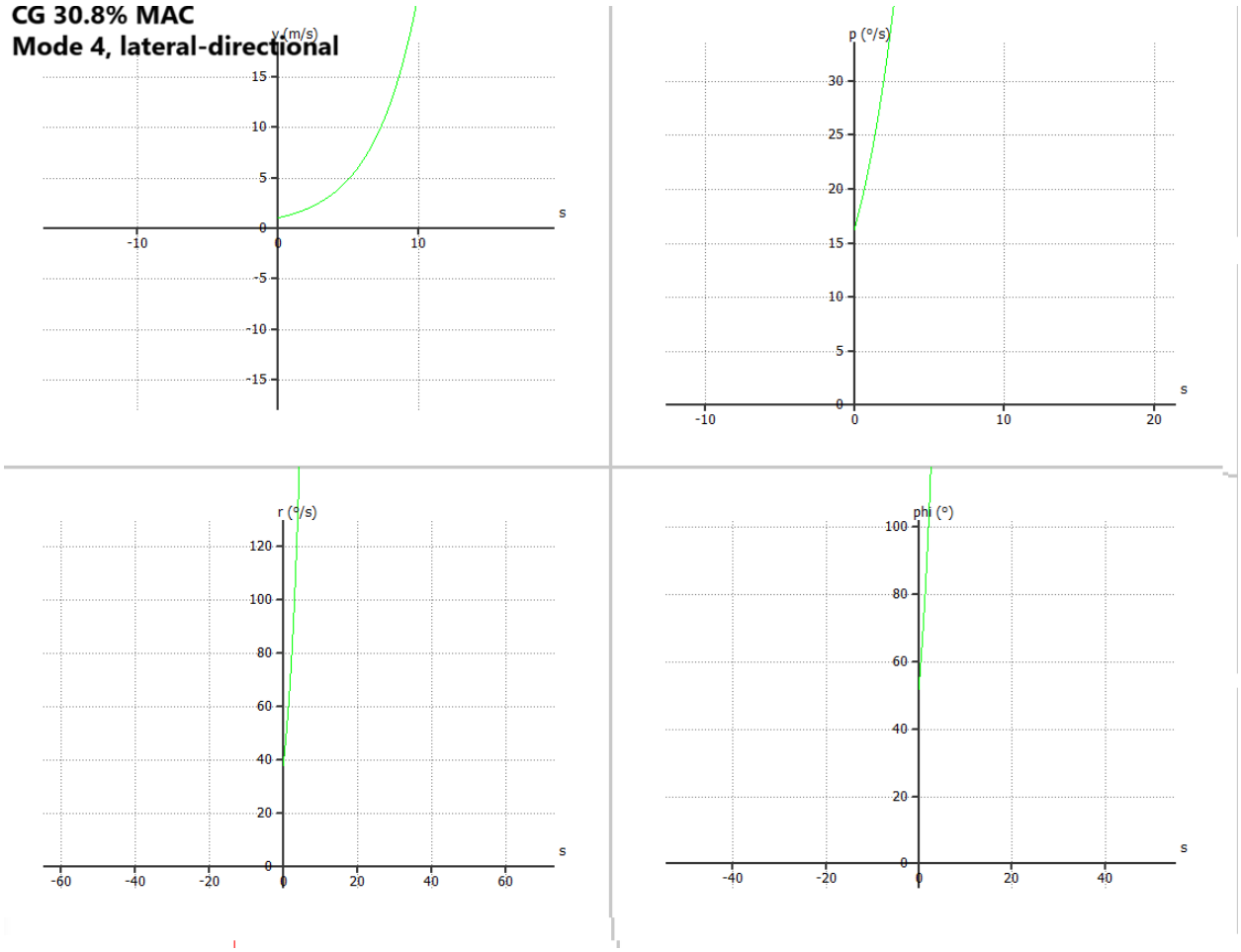

Fig. 24. Mode 4 for CG 30.8% MAC, lateral-directional

At CG 30.8% MAC, the spiral mode (Mode 4) is represented by a purely real positive eigenvalue $\lambda = +0.207$, indicating the same weak divergence as in previous two cases.

$t_{30.8,2x}$ = ln2/0.207 = **3.35 sec**
$t_{30.8,10x}$ = ln10/0.207 = **11.12 sec**

The aircraft is dynamically unstable at spiral mode on all CG locations. The slowest tendency to diverge is noticed at CG = 30.8%.

Overall, the benchmark UAV demonstrates satisfactory static and dynamic stability within the selected CG envelope of **25.8–30.8% MAC**. The aircraft is longitudinally statically stable over the analysed *AOA* range and the short-period mode remains strongly stable and well damped for all CG cases reaching equilibrium response within less than 2 seconds, which indicates a very strong pitch rate damping. The phugoid mode is also dynamically stable at all CG positions, with nearly unchanged natural frequency but it is lightly damped, resulting in long recovery times (92–165 s to 10% amplitude), which is typical for small fixed-wing UAVs. However, this should be considered for manual flight and supports the recommendation to use an autopilot or speed/pitch control for improved long-period damping. In lateral-directional dynamics roll subsidence is extremely fast and stable, and Dutch roll remains stable and well damped across all CG positions, with the oscillation amplitude going to 10% in about 1 second and to 1% in about 2 seconds. The only unfavorable tendency is the spiral mode, which is weakly divergent (positive real eigenvalue) for all investigated

CG positions. But nevertheless, the divergence rate is relatively slow and can be readily counteracted by small corrective inputs or basic autopilot stabilization, making it acceptable for the intended UAV class. However, it is better not to leave control surfaces for a long period of time.

9. Static Stability Validation in Ansys Fluent

It is important to validate if the values obtained in FLOW5 as FLOW5 is considered to be a low-fidelity CFD. For that reason a high-fidelity CFD Ansys Fluent (Student Version) is used [30][37]. Lift coefficient and pitching moment coefficient will be obtained at velocity of 20 m/s with a CG of 25.8%.

A similar validation approach can be found in previous UAV aerodynamic studies. Dantsker and Vahora compared low-order aerodynamic tools such as XFLR5 and AVL with the high-order CFD tool Ansys Fluent for a fixed-wing unmanned aircraft and evaluated lift, drag and pitching moment characteristics. Therefore, the use of Ansys Fluent as a high-fidelity supporting CFD tool for checking the aerodynamic and stability trends obtained from a lower-order tool is considered appropriate for preliminary UAV stability analysis [42].

The flow motion is generally governed by the Navier-Stokes equations, which describe the relationship between velocity, pressure, density and viscosity in a moving fluid [43]. In simplified form it can be written as:

$$\nabla \cdot v = 0. \tag{16}$$

This is the first equation of the continuity for incompressible flow. It states that the velocity field has zero divergence, meaning that there is no net mass accumulation inside a fluid element.

After disclosing Nabla operator:

$$\frac{\partial u}{\partial x} + \frac{\partial v}{\partial y} + \frac{\partial w}{\partial z} = 0,$$

where u, v, w are velocity components along x, y and z directions respectively.

The second equation can be seen below:

$$\rho \left(\frac{\partial v}{\partial t} + v \cdot \nabla v \right) = -\nabla p + \mu \nabla^2 v. \tag{17}$$

The second equation represents the momentum equation of the incompressible Navier–Stokes equations. The left side describes the inertial acceleration of the fluid, where $\partial v/\partial t$ is the local time-dependent acceleration and $v \cdot \nabla v$ is the convective acceleration caused by the motion of the fluid through the velocity field. The right-hand side includes the pressure gradient term $-\nabla p$ and the viscous diffusion term $\mu \nabla^2 v$. Therefore, this equation describes how the velocity field changes under the influence of pressure forces and viscous effects.

The k-ω SST turbulent model was selected because it is suitable for external aerodynamic simulations where boundary layer behaviour, adverse pressure gradients and possible flow separation may affect lift, drag and pitching moment and it is mostly used for the UAVs similar to the benchmark one [44,45].

The benchmark geometry was built in CATIA and imported into Ansys. An enclosure with dimensions of 5000 mm x 5000 mm x 5000 mm was built and set as a computational domain which is a cube of air surrounding the aircraft.

Meshing properties are as not to exceed the Student Version limit of 1000000 cells. The mesh element face size for UAV was selected of 0,02 m each and for the computational domain of 0,4 m. The total number of elements is 865314.

Meshing of the UAV's faces can be seen on Fig. 25 below.

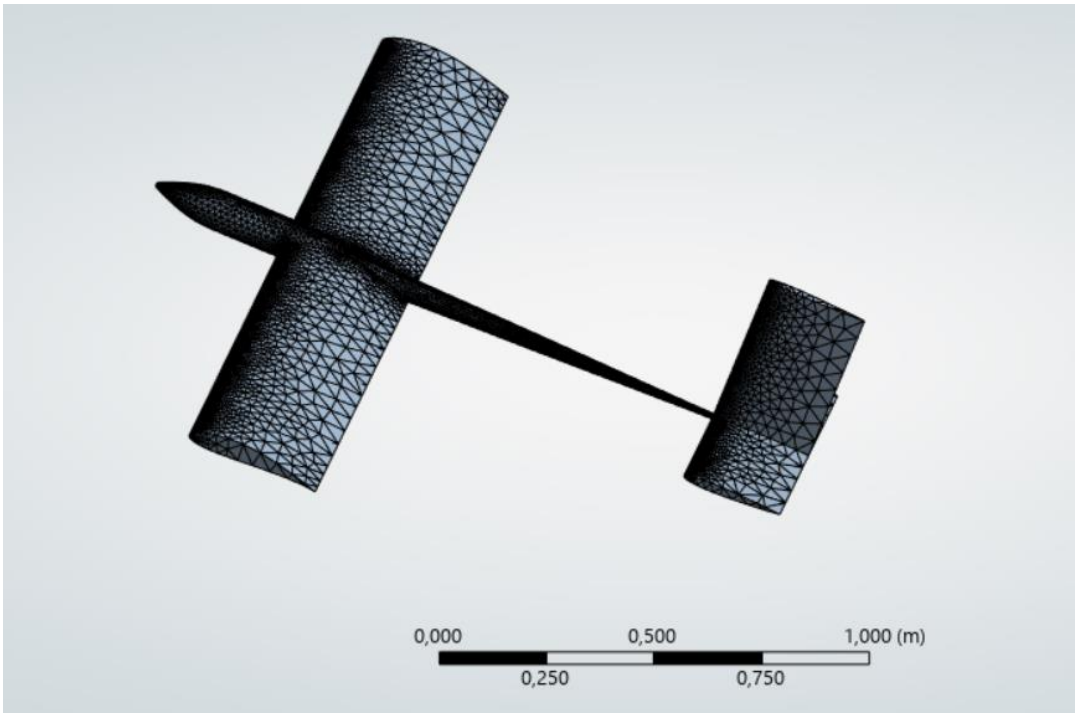

Fig. 25. UAV mesh in Ansys

Boundary conditions are:
Inlet velocity: 20 m/s
Density: 1.25 kg/m³
Enthalpy: 0 J/kgC
Temperature: 288.16 K
Viscosity: $1.7894*10^{-5}$ kg/(m·s)
Ratio of Specific Heats: 1.4
Yplus for Heat Tran. Coef: 300
Center of gravity: 25.8% MAC

The turbulent model used is k-ω SST[36,38].

The case with velocity of 20 m/s and CG of 25.8% is calculated for the following *AOA*: -6, -4, -2, 0, 2, 4, 6, 8, 10.

Lifting forces, drag forces and pitching moments are received as results for each angle of attack. For each parameter (L, D, M) for each *AOA* 300 iterations were performed. An example of successful Lift force iterations report from Ansys Fluent can be seen on Appendix 4 with *AOA* of 10° as an example.

The dynamic pressure can be identified by the following equation [41]:

$$q = \frac{1}{2}\rho v^2 \tag{18}$$

$q = 0.5 \cdot 1.25 \cdot 20^2 = 250\ Pa$

If dynamic pressure is multiplied by the surface wing area then[31]:

$qS = 250 \cdot 0.64 = 160\ N$

Lift coefficient can be found by the equation below [41]:

$$C_L = \frac{L}{qS}. \tag{19}$$

Pitching moment coefficient can be found by the following equation [41]:

$$C_m = \frac{M_z}{qSc}. \tag{20}$$

Knowing mentioned above the Table 4 of identifying the needed coefficients C_L and C_m can be filled. The average values of the results from the iterations are used.

Table 4. C_L and C_m identification from L and M_z

L	$-M_z$	C_L	C_m
-9.97668	-7.56432	-0.062	0,132
17.2834	-2.85226	0.108	0,083
45.0639	1.95706	0.282	0,032
72.0685	6.90591	0.450	-0,02
98.6623	11.5484	0.617	-0,071
124.542	15.717	0.778	-0,112
150.627	20.289	0.941	-0,161
176.371	24.4964	1.102	-0,202
201.147	29.6176	1.257	-0,264

Residual convergence history after Ansys Fluent iterations can be seen on Appendix 3.

The averaged results values are compared to results obtained in FLOW5 and shown on Table 5.

Table 5. Ansys validation results vs FLOW5 results

CFD	*AOA*								
	-6°	-4°	-2°	0°	2°	4°	6°	8°	10°
C_L value on C_L vs *AOA* curve									
FLOW5	-0.025	0.142	0.305	0.473	0.636	0.807	0.965	1.119	1.276
Ansys	-0.062	0.108	0.282	0.45	0.617	0.778	0.941	1.102	1.257
C_m value on C_m vs *AOA* curve									
FLOW5	0.154	0.115	0.075	0.033	-0.006	-0.046	-0.087	-0.125	-0.167
Ansys	0.132	0.083	0.032	-0.02	-0.071	-0.112	-0.161	-0.202	-0.264
Difference Ansys vs FLOW5									
$\|\Delta C_L\|$	0.037	0.034	0.023	0.023	0.019	0.029	0.024	0.017	0.019
$\|\Delta C_m\|$	0.022	0.032	0.043	0.053	0.065	0.066	0.074	0.077	0.097

Difference between C_L vs *AOA* graphs between FLOW5 and Ansys can be seen on Fig. 26.

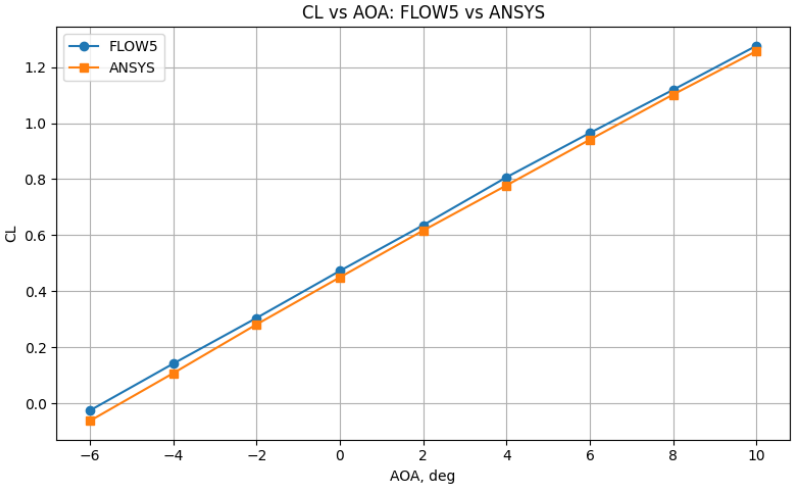

Fig. 26. C_L vs *AOA* comparison between FLOW5 and Ansys

From Fig. 26 it is seen that Ansys shows slightly less values compared to FLOW5 but the slope angle is nearly the same.

Difference between C_m vs *AOA* graphs between FLOW5 and Ansys can be seen on Fig. 27.

The curves have a tendency slightly to converge at the lowest negative *AOA* of -6°, and moving from -6° to +10° the diverging tendency can be seen with a maximum difference of 0.097 at *AOA* of 10°.

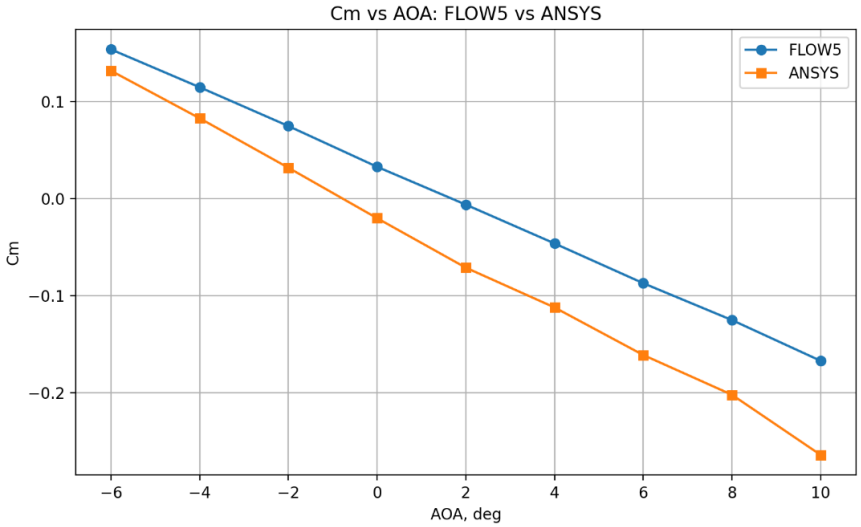

Fig. 27. C_m vs *AOA* comparison between FLOW5 and Ansys

It can be seen that $\frac{\partial C_m}{\partial \alpha} < 0$ meaning that the UAV is statically stable.

C_m vs C_L comparison between FLOW5 and Ansys can be seen on Fig. 28. The smallest difference can be seen in the same way as with C_m vs *AOA*, at lower C_L the converging tendency can be noted while at higher C_L the situation is opposite and the biggest difference achieved at C_L of 1.26.

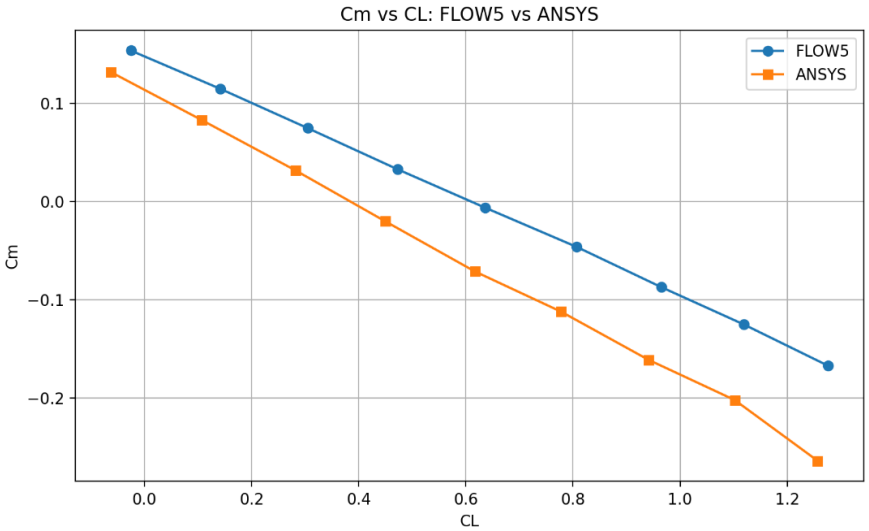

Fig. 28. C_m vs C_L comparison between FLOW5 and Ansys

As the C_m vs C_L curve in Ansys does not give the ideal line compared to FLOW5, the mean slope is found taking into account all 9 points. But firstly the local slope for each part of the line is found:

Point 1-2
$\Delta C_m = 0.083 - 0.132 = -0.049$
$\Delta C_L = 0.108 - (-0.062) = 0.170$
$m_{12(\text{ANSYS})} = -0.049 / 0.170 =$ **-0.2882**

Point 2-3

ΔC_m = 0.032 - 0.083 = -0.051

ΔC_L = 0.282 - 0.108 = 0.174

$m_{23(\text{ANSYS})}$ = -0.051 / 0.174 = **-0.2931**

Point 3-4

ΔC_m = -0.020 - 0.032 = -0.052

ΔC_L = 0.450 - 0.282 = 0.168

$m_{34(\text{ANSYS})}$ = -0.052 / 0.168 = **-0.3095**

Point 4-5

ΔC_m = -0.071 - (-0.020) = -0.051

ΔC_L = 0.617 - 0.450 = 0.167

$m_{45(\text{ANSYS})}$ = -0.051 / 0.167 = **-0.3054**

Point 5-6

ΔC_m = -0.112 - (-0.071) = -0.041

ΔC_L = 0.778 - 0.617 = 0.161

$m_{56(\text{ANSYS})}$ = -0.041 / 0.161 = **-0.2547**

Point 6-7

ΔC_m = -0.161 - (-0.112) = -0.049

ΔC_L = 0.941 - 0.778 = 0.163

$m_{67(\text{ANSYS})}$ = -0.049 / 0.163 = **-0.3006**

Point 7-8

ΔC_m = -0.202 - (-0.161) = -0.041

ΔC_L = 1.102 - 0.941 = 0.161

$m_{78(\text{ANSYS})}$ = -0.041 / 0.161 = **-0.2547**

Point 8-9

ΔC_m = -0.264 - (-0.202) = -0.062

ΔC_L = 1.257 - 1.102 = 0.155

$m_{89(\text{ANSYS})}$ = -0.062 / 0.155 = **-0.4000**

Mean local slope in Ansys:

$$\frac{dC_m}{dC_L}(ANSYS) = \frac{-0.2882 - 0.2931 - 0.3095 - 0.3054 - 0.2547 - 0.3006 - 0.2547 - 0.4000}{8} = -0.3008$$

The static margin can be calculated as:

$SM_{\text{ANSYS}} = -\frac{dC_m}{dC_L}$

$SM_{ANSYS} = \mathbf{30.08\%\ MAC}$

Now the neutral point can be calculated as:

$x_{NP,ANSYS} = x_{CG} + SM_{ANSYS}$

$x_{NP,ANSYS} = 25.8 + 30.08 = \mathbf{55.88\%\ MAC}$

For FLOW5 at CG 25.8% static margin:

$SM_{\text{FLOW5}} = -\frac{dC_m}{dC_L} = 0.247$

SM_{FLOW5} = 24.7% MAC

$x_{NP,ANSYS} = x_{CG} + SM_{\text{FLOW5}} = \mathbf{50.5\%\ MAC}$

Difference in SM and NP obtained at CG 25.8% and velocity of 20 m/s between FLOW5 and Ansys:

$\Delta SM = 30.08 - 24.70 = 5.38\%\ MAC$

$\Delta x_{NP} = 55.88 - 50.50 = 5.38\%\ MAC$

Knowing that MAC=0.32 m in metric system that difference can be expressed as:

$DIF\ (m) = \frac{5.38}{100} \cdot 0.32 = 0.0172$ m = **17.2 mm**

Both methods predict a positive static margin, which confirms that the UAV is longitudinally statically stable at the investigated forward CG position. The Ansys Fluent result also confirms the same negative C_m vs C_L slope trend as FLOW5, while small numerical differences are expected due to the different aerodynamic methods used in both tools. The greatest contribution to the difference was most likely caused by the meshing in Ansys.

Conclusions

1. Theoretical basis was researched on mass and balance, static and dynamic stability applicable for UAV as well as the methodology was defined.
2. A benchmark of aircraft was created with the following main requirements:
   MTOM: 5 kg, Max wingspan: 2 m, v_s = 10 m/s = 36 km/h, v_c = 20 m/s = 72 km/h, v_{ne} = 35 m/s = 126 km/h. The geometry of the benchmark was defined.
3. Mass and balance was calculated. Initially CG of 25.1% was taken and NP of 50.8% and SM of 25.7% MAC were established. Static margin limits of 20-25% MAC and CG limits of 25.8%-30.8% MAC were defined.
4. Stability analysis was performed in FLOW5 under ISA conditions and for 3 selected CGs: 25.8%, 28.3% and 30.8% MAC. After obtaining C_m vs *AOA* curves benchmark was found longitudinally statically stable.
5. When performing more detailed stability analysis it was identified that the benchmark is statically and dynamically stable at all longitudinal and lateral modes, it is dynamically stable at Dutch Roll and dynamically unstable at spiral mode.
6. It was identified that the more forward CG is, the better longitudinal stability is. When shifting CG to aft recovery time from Phugoid significantly increases. At 25.8% MAC- 92 sec, 28.3% MAC - 165 sec, 30.8% MAC – 153 sec. CG is within the investigated CG range, the influence of CG position on lateral-directional modes was limited
7. The best stability modes benchmark showed are: short period with a recovery of less than 2 seconds, roll damping with a recovery of less than 0.2 seconds and Dutch Roll with a recovery less than 3 seconds. In phugoid mode the UAV showed acceptable but not optimal performance with a recommendation of autopilot implementation as damping may take from 1.5 till nearly 3 minutes. In spiral lateral-directional mode the aircraft was found dynamically unstable. It is recommended not to leave the control surfaces without any inputs for a long period of time.
8. The Ansys Fluent validation confirmed the same longitudinal static stability trend as FLOW5, since the pitching moment coefficient decreased with increasing lift coefficient. For the investigated CG position of 25.8% MAC, both methods predicted a positive static margin. Difference between the neutral point and static margin is 5.38% MAC which is 17 mm along the aircraft’s longitudinal axis.

List of references

1. Federal Aviation Administration. Weight and Balance Handbook. FAA-H-8083-1B, U.S.Department of Transportation, 2016.
2. Deener, W. Aircraft Weight and Balance. Aviation Supplies & Academics, Newcastle, WA, 2018.
3. Etkin, B., Reid, L. D. Dynamics of Flight: Stability and Control. 3rd ed., John Wiley & Sons, New York, 1996.
4. Nelson, R. C. Flight Stability and Automatic Control. 2nd ed., McGraw-Hill, New York, 1998.
5. Bonnet, F., Barriola, J. Flight Control Systems. Wiley-ISTE, London, 2015.
6. Stevens, B. L., Lewis, F. L. Aircraft Control and Simulation. 2nd ed., John Wiley & Sons, New York, 2003.
7. EASA ATPL Theory – Mass and Balance.
8. A. Deperrois, XFLR5 – Stability Analysis Documentation, 2011
9. University of Seville, XFLR5 Stability and Flight Modes, lecture material
10. L. Morino et al., Mass and Inertia Modeling in XFLR5, academic notes
11. M. Drela, AVL User Primer, MIT, https://web.mit.edu/drela/Public/web/avl/
12. NASA, OpenVSP Overview, https://openvsp.org
13. NASA, OpenVSP Mass Properties Analysis, https://www.nasa.gov/reference/openvsp-massanalysis/
14. OpenVSP Documentation, VSPAERO Stability Analysis
15. USAF, Stability and Control DATCOM, 1976
16. T. Vogeltanz, R. Jašek, Use of Digital DATCOM for UAV Stability Analysis, 2014
17. Introduction to Aircraft Stability (Static & Dynamic) – R.H. Barnard & D.R. Philpott – p. 10 – https://webpage-a360a5.gitlab.io/pdf/5-Stability.pdf
18. Aircraft Stability and Control. Dr. Akeel Ali Wannas – https://me.uotechnology.edu.iq/wpcontent/uploads/2024/12/Aircraft-Stability-and-Control.pdf
19. Flow 5 - https://flow5.tech/flow5.html
20. Deperrois, A. About Stability Analysis Using XFLR5. Revision 2.1, 2010. Available at: https://flow5.tech/xflr5/docs/XFLR5_and_Stability_analysis.pdf [Accessed: 4 May 2026].
21. Campos Rodriguez, V. A., Su, Y. Preliminary Design and Performance-Stability Analysis of a Fixed-Wing UAV Using XFLR5. Journal of Aircraft and Spacecraft Technology, 2023, vol. 7, pp. 8–16. DOI: 10.3844/jastsp.2023.8.16. Available at: https://thescipub.com/abstract/jastsp.2023.8.16 [Accessed: 4 May 2026].
22. Karki, A., Darlami, K., Bhattrai, S. Conceptual Design and Stability Analysis of a Fixed Wing UAS Research Platform for Aerial Experiments. Proceedings of 10th IOE Graduate Conference, 2021. Available at: https://conference.ioe.edu.np/ioegc10/papers/ioegc-10-006-10009.pdf [Accessed: 4 May 2026].
23. Aircraft Design Lecture Notes. Tail Surface Design: Tail Volume Coefficients. Available at: https://webpage-a360a5.gitlab.io/pdf/10-TailSizing.pdf [Accessed: 4 May 2026].
24. Brigham Young University. ME 415 Assignment #4: Stability. 2020. Available at: https://flowlab.groups.et.byu.net/me415/hw/hw4.pdf [Accessed: 4 May 2026].
25. Aircraft Stability and Control. Dr. Akeel Ali Wannas – https://me.uotechnology.edu.iq/wpcontent/uploads/2024/12/Aircraft-Stability-and-Control.pdf

26. M. Peet, Aircraft Dynamics — Lecture 11: Dynamic Stability and Modes, Arizona State University.
27. A. G. Slongo, D. D. Moraes, L. Q. Mantovani, and M. S. Venturini, “Handling Qualities Analysis of an Unmanned Aircraft Vehicle for Agricultural Spraying,” Journal of Aerospace Technology and Management, vol. 12, Special Edition, pp. 38–51, 2020.
28. Sosa Henríquez, C. Preliminary Global Sizing. Stability and Control of Aircrafts, Master’s Program Aeronautical Engineering, Kaunas University of Technology, lecture slides, 2026.
29. Barua, P., Sousa, T., Scholz, D. Empennage Statistics and Sizing Methods for Dorsal Fins. Technical Note, Aircraft Design and Systems Group (AERO), Hamburg University of Applied Sciences, 2013. Available at: https://www.fzt.hawhamburg.de/pers/Scholz/Aero/AERO_TN_TailSizing_13-04-15.pdf [Accessed: 4 May 2026].
30. ANSYS. Ansys Student. Available at: https://www.ansys.com/academic/students
31. Anderson, J. D. Fundamentals of Aerodynamics. 6th ed., McGraw-Hill Education, New York, 2017.
32. McCormick, B. W. Aerodynamics, Aeronautics, and Flight Mechanics. 2nd ed., Wiley, New York, 1995.
33. Raymer, D. P. Aircraft Design: A Conceptual Approach. 6th ed., American Institute of Aeronautics and Astronautics, Reston, VA, 2018. DOI: 10.2514/4.104909.
34. Stengel, R. F. Flight Dynamics. Princeton University Press, Princeton, 2004.
35. Drela, M. XFOIL: An Analysis and Design System for Low Reynolds Number Airfoils. In: Mueller, T. J., ed. Low Reynolds Number Aerodynamics. Lecture Notes in Engineering, vol. 54. Springer, Berlin, Heidelberg, 1989. DOI: 10.1007/978-3-642-84010-4_1.
36. Menter, F. R. Two-equation eddy-viscosity turbulence models for engineering applications. AIAA Journal, 1994, vol. 32, no. 8, pp. 1598–1605. DOI: 10.2514/3.12149.
37. Versteeg, H. K., Malalasekera, W. An Introduction to Computational Fluid Dynamics: The Finite Volume Method. 2nd ed., Pearson Education, Harlow, 2007.
38. ANSYS. Ansys Fluent Theory Guide. Available at: https://ansyshelp.ansys.com/public/Views/Secured/corp/v261/en/pdf/Ansys_Fluent_Theory_Guide.pdf [Accessed: 12 May 2026].
39. Selig, M. S. UIUC Airfoil Coordinates Database. University of Illinois at Urbana-Champaign, Applied Aerodynamics Group. Available at: https://m-selig.ae.illinois.edu/ads/coord_database.html .
40. Abbott, I. H., von Doenhoff, A. E., Stivers, L. S. Summary of Airfoil Data. NACA Report No. 824, National Advisory Committee for Aeronautics, 1945. Available at: https://digital.library.unt.edu/ark:/67531/metadc65534/ .
41. NASA Glenn Research Center. Dynamic Pressure. Beginners Guide to Aeronautics. Available at: https://www1.grc.nasa.gov/beginners-guide-to-aeronautics/dynamic-pressure-2/ .
42. DANTSKER, O. D.; VAHORA, M. Comparison of Aerodynamic Characterization Methods for Design of Unmanned Aerial Vehicles. American Institute of Aeronautics and Astronautics, 2018. Available at: https://uavdb.org/download/avistar/6.2018-0272.pdf
43. NASA Glenn Research Center. Navier-Stokes Equations. Beginners Guide to Aeronautics. Available at: NASA Glenn Research Center website.

44. ALMHEIRI, Z.; ALEID, R.; DOL, S. S. Design of Fixed-Wing and Multi-Copter Hybrid Drone. WSEAS Transactions on Systems, 2021, vol. 20, pp. 31–39. DOI: 10.37394/23202.2021.20.5. Available at: https://wseas.com/journals/systems/2021/a105102-003(2021).pdf
45. İNAN, A. T.; CEYLAN, M. Aerodynamic Analysis of Fixed-Wing Unmanned Aerial Vehicles Moving in Swarm. Applied Sciences, 2024, vol. 14, no. 15, article 6463. DOI: 10.3390/app14156463. Available at: https://www.mdpi.com/2076-3417/14/15/6463

Appendices

Appendix 1. Rule-of-thumb reference values for V_{HTP}

Aircraft Type	Raymer	Roskam	Torenbeek	Howe	Schaufele	Jenkinson	Nicolai
Sailplane	0.500			0.500			
Civil props							
Homebuilts	0.500	0.467					
Personal					0.48-0.92		
GA[a]- Single engine	0.700	0.667		0.650			
GA[a]- Twin engine	0.800	0.786		0.850			
Commuter					0.46-1.07		
Regional Turboprop	0.900	1.075	1.006	1.000	0.83-1.47		
Jet							
Business Jets		0.721	0.691	0.700	0.51-0.99		
Jet transport	1.000	1.010	0.904	1.200	0.54-1.48	0.875	
Supersonic Cruise Airplanes		0.535					
Military							
Jet Trainer	0.700	0.639		0.650			
Jet Fighter	0.400	0.362			0.20-0.75		0.307
Military Transport	1.000	0.891	0.850	0.650			
Special Purpose							
Agricultural	0.500	0.526					
Flying Boat	0.700	0.641					

[a] GA stands for General Aviation

Appendix 2. Rule-of-thumb reference values for V_{VTP}

Aircraft Type	Raymer	Roskam	Howe	Toren. [a]	Schaufele	Jenk. [b]	Nicolai
Sailplane	0.020		0.018				
Civil props							
Homebuilts	0.040	0.036					
Personal					0.024 … 0.086		
GA- single engine	0.040	0.043	0.050				
GA- twin engine	0.070	0.062	0.065				
Commuter					0.041 … 0.097		
Regional Turboprop	0.080	0.083	0.080	0.077	0.065 … 0.121		
Jet							
Business Jets		0.073	0.065	0.069	0.061 … 0.093		
Jet transport	0.090	0.079	0.090	0.074	0.038 … 0.120	0.076	
Supersonic Cruise Airplanes		0.062	0.065				
Military							
Military Trainer	0.060	0.061	0.065				
Military Fighter	0.070	0.077			0.041 … 0.130		0.064
Military Transport	0.080	0.073	0.065				
Special Purpose							
Agricultural	0.040	0.032					
Flying Boat	0.060	0.050					

[a] Toren. stands for the author Torenbeek
[b] Jenk. stands for the author Jenkinson

Appendix 3. Residual convergence history after Ansys Fluent iterations

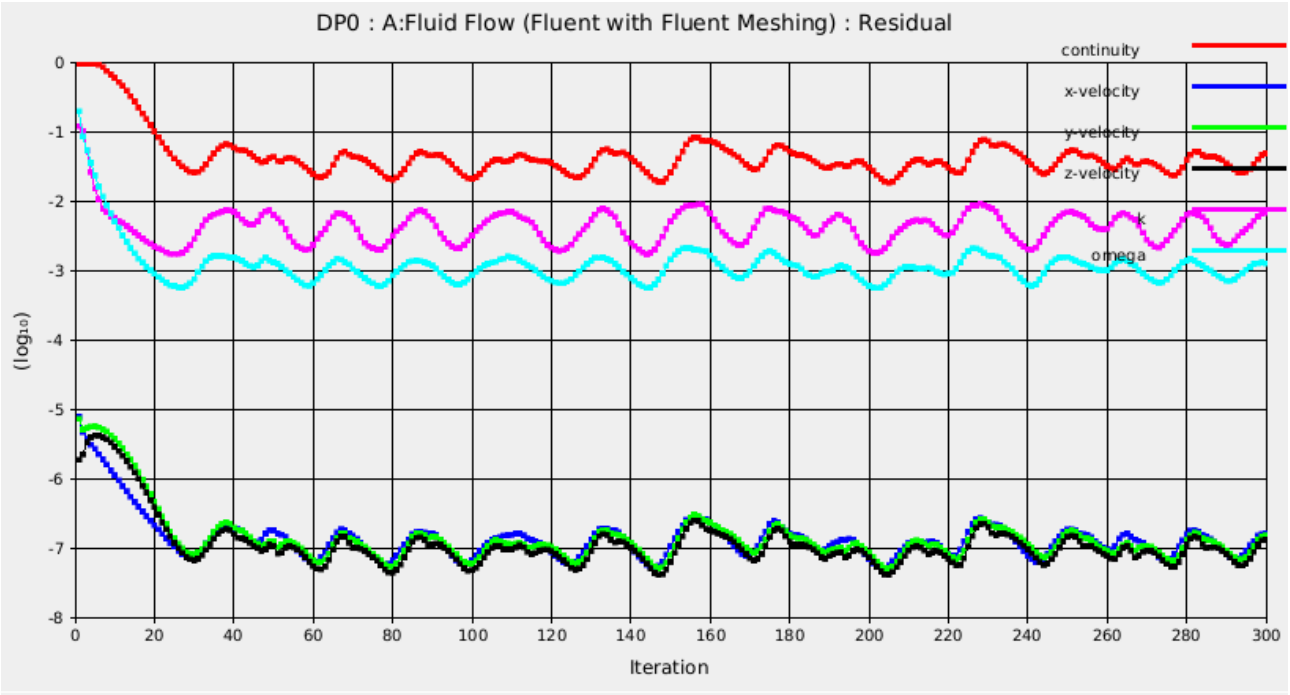

Appendix 4. Lift force iterations monitor of Ansys Fluent at *AOA* = 10°